Natural Resources Canada | Ressources naturelles Canada

GEOLOGICAL SURVEY OF CANADA
OPEN FILE 8751

Geomorphologic feature mapping methodology developed for the Dempster Highway and Inuvik to Tuktoyaktuk Highway corridors

W.E. Sladen, R.J.H. Parker, S.V. Kokelj, and P.D. Morse

2021

Canada

GEOLOGICAL SURVEY OF CANADA
OPEN FILE 8751

Geomorphologic feature mapping methodology developed for the Dempster Highway and Inuvik to Tuktoyaktuk Highway corridors

W.E. Sladen[1], R.J.H. Parker[1], S.V. Kokelj[2], and P.D. Morse[1]

[1]Geological Survey of Canada, 601 Booth Street, Ottawa, Ontario
[2]Northwest Territories Geological Survey, 4601-B 52nd Avenue, Yellowknife, Northwest Territories

2021

Permanent link: https://doi.org/10.4095/328181

This publication is available for free download through GEOSCAN (https://geoscan.nrcan.gc.ca/).

Recommended citation
Sladen, W.E., Parker, R.J.H., Kokelj, S.V., and Morse, P.D., 2021. Geomorphologic feature mapping methodology developed for the Dempster Highway and Inuvik to Tuktoyaktuk Highway corridors; Geological Survey of Canada, Open File 8751, 1 .zip file. https://doi.org/10.4095/328181

Publications in this series have not been edited; they are released as submitted by the author.

ABSTRACT

Thaw of permafrost and associated ground ice can reduce ground stability, modify terrain, and reconfigure drainage patterns. This, in turn, can affect terrestrial and aquatic ecosystems, and present challenges to northern societies. Permafrost change can have a significant influence on the integrity of ground-based transportation infrastructure, which is critical to northern communities. The geomorphic landscape can indicate ground ice presence and thaw susceptibility.

In 2017, the Geological Survey of Canada and the Northwest Territories Geological Survey collaboratively developed a robust methodology to classify and digitize geomorphic features in permafrost terrain using high-resolution imagery. A 10-km wide corridor centred on the Dempster Highway and Inuvik to Tuktoyaktuk Highway was used to develop and test the methodology. The 875-km-long corridor traverses a variety of geological and physiographic terrain types, including glaciated and non-glaciated terrain. Permafrost here is continuous. However, variation in climate, relief, ecology, and disturbance have produced a diverse range of periglacial conditions. We selected five test sections representative of terrain along the study corridor. The main geomorphic categories are mass movement, hydrological, and periglacial. We used high-resolution (0.6 m) satellite imagery to generate stereo pairs for 3D visualization. Geomorphic features were digitized in ArcGIS. We customized Python scripts to populate the attributes for each geomorphic feature. This Open File provides a background on the physical context and physiographic terrain of the study corridor. The report presents the geomorphic feature identification and digitization methodology and summarizes the results from the test section mapping and its limitations.

DISCLAIMER

Her Majesty the Queen in right of Canada, as represented by the Minister of Natural Resources ("Canada"), does not warrant or guarantee the accuracy or completeness of the information ("Data") and does not assume any responsibility or liability with respect to any damage or loss arising from the use or interpretation of the Data.

The Data are intended to convey regional trends and should be used as a guide only. The Data should not be used for design or construction at any specific location, nor are the Data to be used as a replacement for types of site-specific geotechnical investigations.

TABLE OF CONTENTS

LIST OF FIGURES

LIST OF TABLES

1 INTRODUCTION

In operation since 1979, the 737-km-long Dempster Highway (DH) starts at the junction with the Klondike Highway near Dawson, Yukon and ends in Inuvik, Northwest Territories. The recently (2017) opened 138-km-long Inuvik to Tuktoyaktuk Highway (ITH) provides road access to the Beaufort-Delta region in Canada's western Arctic (Figure 1). Together, these highways are Canada's northernmost all-season road corridor. The combined 875-km-long corridor traverses a variety of surficial geology and physiographic regions including glaciated and non-glaciated terrain (Bostock, 1970; Mathews, 1986; Rampton, 1988; Roots and Hart, 2004). Permafrost is continuous throughout 91% of the corridor, but permafrost conditions are highly variable due to varied relief, climate, vegetation, forest fire regimes, and landscape histories (Heginbottom *et al.*, 1995; Burn, 2004; Burn and Kokelj, 2009; Burn *et al.*, 2015; Kokelj *et al.*, 2017a; O'Neill *et al.*, 2019). Thaw of permafrost and associated ground ice reduces ground stability, modifies terrain, and reconfigures drainage patterns, which can affect terrestrial and aquatic ecosystems and present challenges to northern societies (Vincent *et al.*, 2012). In particular, changing permafrost conditions can have a significant influence on the integrity of ground-based transportation infrastructure, which is critical to northern communities (Nelson *et al.*, 2001; Callaghan *et al.*, 2011). The DH-ITH corridor provides a societally-relevant landscape transect for conducting multidisciplinary research on permafrost thermal conditions, terrain sensitivity, and climate change impacts on terrain and infrastructure.

In 2017, the Geological Survey of Canada (GSC) of Natural Resources Canada, and the Northwest Territories Geological Survey (NTGS) began a collaborative project to map permafrost terrain. A key aspect of this project is to develop a robust classification scheme and mapping methodology to digitize geomorphic features using recent high-resolution imagery. The method involves using a 10-km-wide corridor centred on the DH-ITH alignment to develop and test the classification scheme and mapping methodology. The geomorphic categories include mass movement, periglacial, and hydrological features. The goal is to develop a permafrost classification scheme and mapping methodology that can be utilized in future permafrost, geohazard, and thermokarst maps.

This Open File presents the feature classification scheme and digitizing methodology developed based on select locations along the DH-ITH. The custom Python® script is included in the Appendices. The digitizing results of five corridor test sections are summarized. This Open File is part of a larger initiative to identify and digitize periglacial, hydrological, and mass movement geomorphic features along the entire 10-km-wide DH-ITH corridor and to provide a data set to support modeling thaw susceptibility of permafrost terrain (e.g., Rudy *et al.*, 2019).

2 PHYSICAL CONTEXT

The DH-ITH study corridor is located in northwestern Canada (Figure 1). The Dempster Highway starts in west-central Yukon at 64°N and traverses the mountainous Northern Cordillera terrain of the Ogilvie Mountains, Eagle Plain upland, and Richardson Mountains, which ranges in elevation from 330 m asl at the Eagle River to 1324 m asl in the Southern Ogilvie Mountains (Figure 1 and 2). At km 463, the DH corridor crosses the Northwest Territories border and traverses the Peel Plateau upland (maximum elevation 494 m asl) before descending onto the low-lying Peel and Anderson plains of the Interior Plain (elevation range 6 to 106 m asl) and terminating in Inuvik at 68.4°N. The ITH corridor continues northward from Inuvik over the Anderson Plain and the Tuktoyaktuk Coastlands before ending at the Beaufort Coast at 69.4°N latitude. The ITH corridor terrain is low-lying with elevations ranging from 152 m asl in the Caribou Hills near Inuvik to sea level at Tuktoyaktuk.

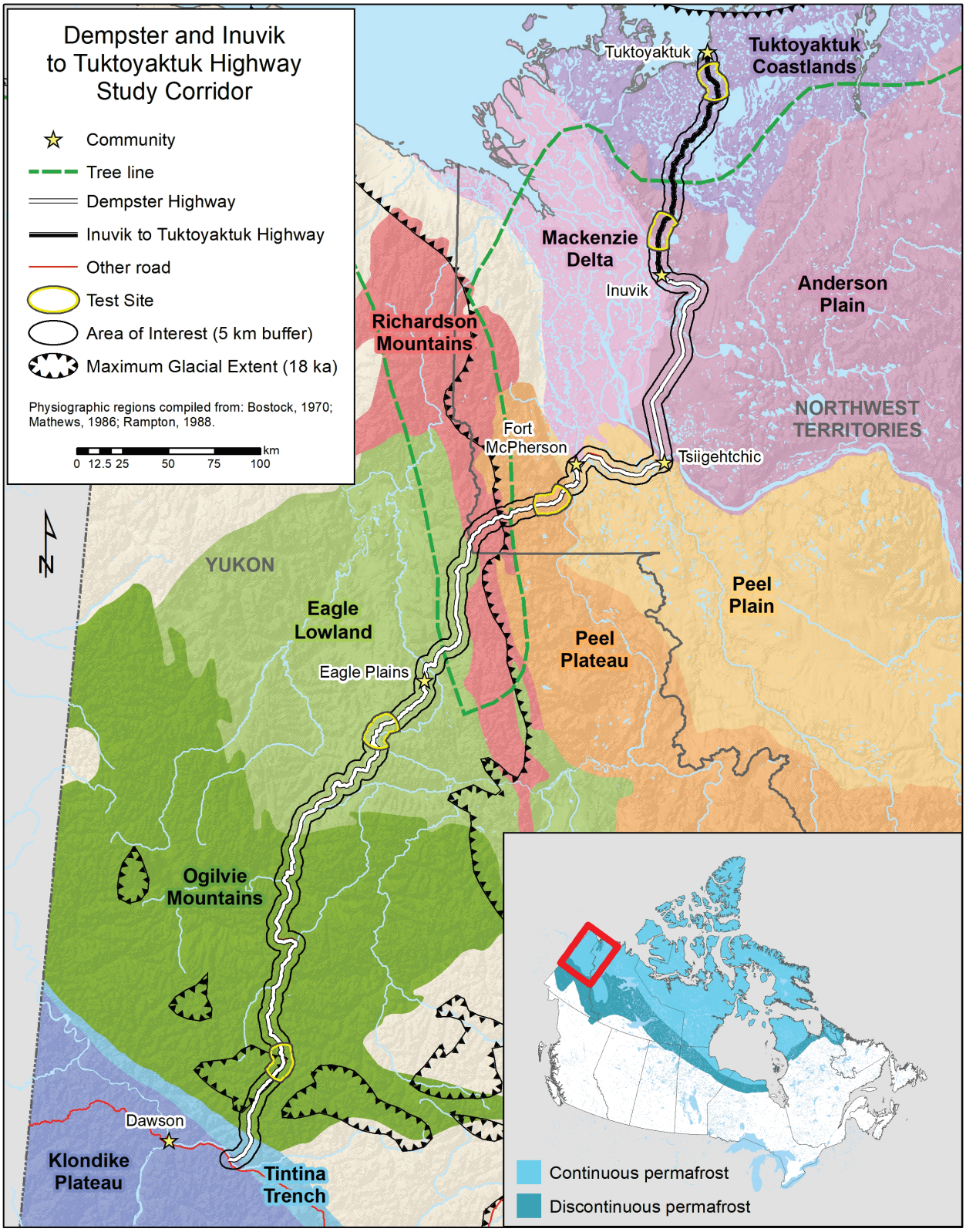

Figure 1. Location of the study corridor, extent of glaciated terrain, and physiographic regions. Test areas are indicated in yellow. Maximum glacial extent from Gordey and Makepeace (2003). Shaded relief from USGS (2007). Inset shows extent of main map and continuous and discontinuous permafrost zones (Heginbottom *et al.*, 1995).

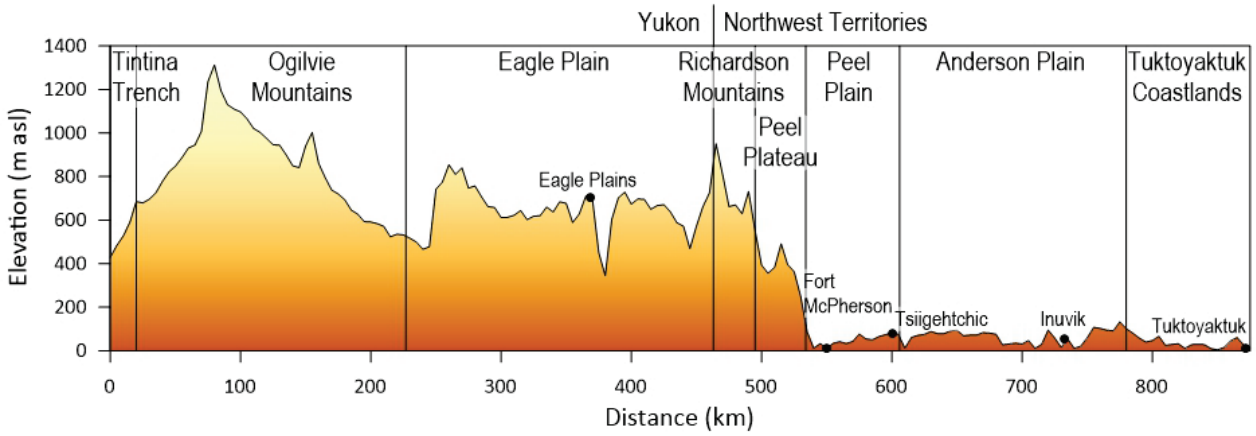

Figure 2. Elevation profile of the Dempster and Inuvik to Tuktoyaktuk highways. Elevations are at 5-km intervals. The locations of the physiographic regions, communities, and territorial border along the study corridor are shown.

2.1 Geology and Glacial History

In the northern Canadian Cordillera, the bedrock is uplifted ocean floor deposits consisting of sandstones, shales, and limestones (Roots and Hart, 2004). Beneath the Interior Plains, the bedrock is clastic and carbonate sedimentary rock, consisting mainly of sandstone and shale (Dixon *et al.*, 1992). Glaciation has been variable along the study corridor. The central portion of the DH (km 116-495) passes through unglaciated terrain, resulting in a surficial geology dominated by weathered bedrock and colluvial sediments (Figure 1). The southern portion of the DH (km 75-116) experienced valley glaciation during the Wisconsinan period, whereas the remainder of the corridor northwest of km 495 experienced continental glaciation and was covered by the Laurentide Ice Sheet (Burn and Kokelj, 2009; Burn *et al.*, 2015). The latter area is covered with till, glaciolacustrine, and glaciofluvial deposits (Burn and Kokelj, 2009; O'Neill *et al.*, 2015).

2.2 Climate

The climate south of treeline is subarctic continental, whereas north of the forest-tundra transition the climate is arctic coastal (Rampton, 1988; Burn *et al.*, 2015). Throughout the region, the winters are long and cold, with mean January temperatures of -27.0 °C. Summers are short and cool, with mean July temperatures ranging from 15.7 °C at Dawson to 11.0 °C at Tuktoyaktuk. Mean annual air temperatures range from -4.1 °C to -10.1 °C, decreasing towards the coast (Table 1) (Environment Canada, 2020). In mountainous terrain, winter temperatures are commonly colder in the valleys due to topographic shading and cold-air drainage (Lewkowicz *et al.*, 2012; O'Neill *et al.*, 2015). Total annual precipitation varies from 324 mm at Dawson to 161 mm at Tuktoyaktuk, of which 51-64% falls as snow.

Table 1. Climate normal (1981-2010) mean annual air temperature (MAAT), total annual rainfall, and total annual snowfall data from Environment Canada meteorological stations along the DH-ITH corridor (Environment Canada, 2020).

Station	km	Latitude (°N)	Longitude (°W)	Elevation (m)	MAAT (°C)	Rainfall (mm)	Snowfall (cm)
Dawson	0	64.04	139.13	346	-4.1	201.3	166.5
Fort McPherson	550	67.41	134.86	22	-7.3	145.9	152.5
Inuvik	732	68.30	133.48	15	-8.2	114.5	158.6
Tuktoyaktuk	875	69.43	133.03	0	-10.1	74.9	103.1

2.3 Permafrost

The DH-ITH corridor is almost completely within the continuous permafrost zone (Heginbottom *et al.*, 1995). Permafrost thickness ranges from 20 to 60 m near Dawson and 89 m in the Eagle Plain to 400 m north of Inuvik (Rampton, 1988; Burn, 2004), although thickness may vary locally with proximity to water bodies. Active-layer thickness ranges from 40 to 150 cm and mean annual ground temperatures range from -1.2 to -6.6 °C (Burn and Kokelj, 2009; Burn *et al.*, 2015). Ground ice is present as buried glacial ice, wedge ice, syngenetic segregated ice, and intrusive ice (Burn *et al.*, 2015; O'Neill *et al.*, 2019). Features indicative of ground ice, including ice-wedge polygons, retrogressive thaw slumps, and pingos, are observed throughout the corridor.

3 PHYSIOGRAPHIC REGIONS

The DH-ITH corridor extends from the unglaciated portion of the Cordilleran physiographic region in the Yukon to glaciated Interior Plain and Arctic Coastland physiographic regions in the Northwest Territories (Figure 1) (Bostock, 1948). The physiographic subdivisions traversed by the DH-ITH corridor from south to north are summarized below.

3.1 Cordilleran Region

3.1.1 Klondike Plateau (DH 0 to 4 km)

The mostly unglaciated Klondike Plateau is characterized by a dendritic pattern of deep, narrow, V-shaped valleys and long, smooth-topped ridges and mountains of mainly uniform elevation (Bostock, 1948; Green, 1972; Scudder, 1997). The bedrock primarily consists of metamorphosed Paleozoic and Precambrian sedimentary rocks, dominantly quartzite, quartz-mica schist, and marble, and minor granitic and volcanic rocks of the Yukon-Tanana Terrane (Smith *et al.*, 2004). These rocks are overlain by Tertiary volcanic and sedimentary rocks (Bostock, 1948). The surficial geology is characterized by felsenmeer at higher elevations and colluvial veneer that thickens downslope (Thomas and Rampton, 1982a; Smith *et al.*, 2004). Permafrost is extensive, especially on north-facing slopes, and has a low to moderate amount of ground ice (Heginbottom *et al.*, 1995; Smith *et al.*, 2004; O'Neill *et al.*, 2019). The alpine treeline varies from 1000 to 1200 m asl with alpine tundra vegetation existing above treeline. Below the treeline black spruce (*Picea mariana*) forest exists on the cooler north-facing slopes where permafrost is present with mixed forests growing on the warmer south-facing slopes (Smith *et al.*, 2004).

3.1.2 Tintina Trench (DH 4 to 20 km)

The Tintina Trench is a straight, steep-sided valley with a relatively flat floor that trends northwest-southeast across the centre of the Yukon (Thomas and Rampton, 1982a; Scudder, 1997). The valley bottom varies from 4.8 to 22.5 km in width and 425 to 823 m asl in elevation (Scudder, 1997). A

major extinct fault, the Tintina Trench separates the relatively metamorphosed rocks of the Klondike Plateau to the southwest from the relatively unmetamorphosed sedimentary rocks to the east (Green, 1972; Smith *et al.*, 2004). The surficial geology of the valley consists of alluvial plains and terraces as well as glacial outwash terraces at the mouth of the North Klondike River with colluvium and aeolian deposits dominating the slopes (Thomas and Rampton, 1982a). Permafrost is extensive, but absent beneath major rivers and on some south-facing slopes. Heginbottom *et al.* (1995) and O'Neill *et al.* (2019) predict ground ice amount to be low to moderate in this region. Boreal forest and wetlands cover the valley and are frequently affected by forest fires, resulting in the majority of vegetation being less than 100 years old (Smith *et al.*, 2004).

3.1.3 Ogilvie Mountains (DH 20 to 227 km)

The Ogilvie Mountains consist of steep, sharp peaks and ridges, reaching 2193 m asl at Tombstone Mountain, but the regional relief ranges from 750 to 1500 m (Bostock, 1970; Smith *et al.*, 2004). Alpine and valley glaciers during the Pleistocene produced steep-sided U-shaped valleys (Bostock, 1970; Thomas and Rampton, 1982a). The bedrock geology is comprised almost entirely of sedimentary rock with the addition of intrusive rocks in the southern portion (Bostock, 1948; Smith *et al.*, 2004). The surficial geology is predominately colluvium of varying thickness and texture (Thomas and Rampton, 1982a; 1982b; 1982c, 1982d). Permafrost is extensive in the southern portion and continuous permafrost throughout the central and northern portions of the region with a low to moderate amount of ground ice (Heginbottom *et al.*, 1995; O'Neill *et al.*, 2019). The vegetation is alpine tundra with taiga forest in valleys below 1200 m asl in the south, and 900 m asl in the north (Smith *et al.*, 2004).

3.1.4 Eagle Plain (DH 227 to 463 km)

The unglaciated Eagle Plain or Lowlands is characterized by long, evenly-topped ridges with rounded summits up to about 275 m asl (Bostock, 1970). The incised sedimentary basin consists of broadly-folded shales, sandstones, siltstones, and limestone of Middle Cambrian to Tertiary age (Richardson and Sauer, 1975). Colluvial and alluvial deposits derived from fractured bedrock blanket the slopes (Richardson and Sauer, 1975; Thomas and Rampton, 1982d; 1982e; 1982f; Smith *et al.*, 2004). Permafrost is continuous and ground ice content is variable (Heginbottom *et al.*, 1995; O'Neill *et al.*, 2019). The vegetation is predominately black spruce below treeline (735 m asl) and shrub tundra at higher elevations (Richardson and Sauer, 1975).

3.1.5 Richardson Mountains (DH 463 to 495 km)

The unglaciated southern ranges of the Richardson Mountains are characterized by smooth, flat to rounded mountain tops, steep slopes, and narrow gullies (Bostock, 1970; Thomas and Rampton, 1982e). Relief ranges from 450 to 900 m with elevations reaching over 1600 m asl (Smith *et al.*, 2004). The southern Richardson Mountains are a northward-plunging anticline of sandstone and limestone (Richardson and Sauer, 1975; Thomas and Rampton, 1982e; Norris, 1997; Smith *et al.*, 2004). The summits and upper mountain slopes are blanketed with rock fragments, felsenmere, and colluvium from mass wasting and weathering (Smith *et al.*, 2004). Fans and pediment slopes, formed by weathered rock and by soliflucted and colluviate materials, are found at lower elevations (Thomas and Rampton, 1982f; Duk-Rodkin and Hughes, 1992a; Smith *et al.*, 2004). Permafrost is continuous (Heginbottom *et al.*, 1995). O'Neill *et al.* (2019) predict medium to high amounts of ground ice content with near-surface aggradational ice present in alluvial fans and as ice wedges along the pediments (Richardson and Sauer, 1975; Smith *et al.*, 2004). Mean annual ground temperatures (MAGTs) are about -3.6 °C and -3.8 °C (Burn *et al.*, 2015; Idrees *et al.*, 2015). The Richardson

Mountains are dominated by shrub and tussock tundra, with forest limited to valleys at elevations below 600 m asl (Smith *et al.*, 2004).

3.2 Interior Plains

3.2.1 Peel Plateau (DH 495 to 534 km)

The glaciated Peel Plateau is a fluvially-incised, ice-rich moraine landscape along the eastern margins of the Richardson and Mackenzie Mountains (Kokelj *et al.*, 2017a). The Peel Plateau slopes gently eastward from 750 m asl at the foothills of the Richardson Mountains to 100 m asl west of the Peel River (Catto, 1996). Surficial materials are mainly ice-rich tills, glaciolacustrine, and glaciofluvial deposits up to 50-m thick (Duk-Rodkin and Hughes, 1992a). Cretaceous marine shales and siltstones comprise the bedrock, which is only exposed on the steep slopes or bottoms of incised stream valleys (Norris, 1984; Kokelj *et al.*, 2017a). The continuous permafrost extends to 125-m depth and is predicted to contain a medium to high amount of ground ice (Mackay, 1967; Heginbottom *et al.*, 1995; O'Neill *et al.*, 2019). The annual mean temperature of permafrost increases with elevation from about -2.5 °C in lowland subarctic forest to about -1.5 °C in upland dwarf shrub tundra due to atmospheric inversions in winter (O'Neill *et al.*, 2015). The ice-rich permafrost consists of icy diamicton overlying relict massive ice and icy sediments of segregated origin up to tens of metres in thickness (Lacelle *et al.*, 2004; Malone *et al.*, 2013). Limited wedge ice is present in organic deposits (Kokelj *et al.*, 2017a). Solifluction, active-layer detachment detachments, and retrogressive thaw slumps are common throughout the region.

3.2.2 Peel Plain (DH 534 to 606 km)

The Peel Plain, located between the Peel and Mackenzie Rivers, is characterized by relatively flat, low-lying terrain, approximately 122 m asl, with numerous lakes, fens, and peatlands (Bostock, 1970; Duk-Rodkin and Hughes, 1992a). Hummocky and rolling moraine up to 20-m thick and isolated fen and peatlands 2- to 4-m thick overlie Devonian and Carboniferous sandstone and shale (Norris, 1984; Duk-Rodkin and Hughes, 1992a; 1992b). Permafrost is continuous, up to 100-m thick and is generally ice rich (Heginbottom *et al.*, 1995; Burn and Kokelj, 2009; O'Neill *et al.*, 2019). Annual mean permafrost temperature recorded near Fort McPherson is -2.6 °C (O'Neill *et al.*, 2015). Ground ice occurs in polygonal peatlands as wedge ice and pore ice, and as segregated ice lenses in glaciolacustine sediments and till (Duk-Rodkin and Hughes, 1992a; Kokelj *et al.*, 2014). The vegetation is dominated by open black spruce-lichen forest, lichen and scattered black spruce on peat plateau bogs (Ecosystem Classification Group, 2007).

3.2.3 Anderson Plain (DH 606 to 725 km, ITH 12 to 40 km)

The Anderson Plain, north of the Mackenzie River, is characterized by gently sloping terrain with an average elevation of 225 m asl (Duk-Rodkin and Hughes, 1992b). South of Inuvik, the rolling plain consists of till, 1- to 3-m thick, and organic peatlands overlying Cretaceous and Devonian shales, sandstones, and siltstones (Norris, 1984; Duk-Rodkin and Hughes, 1992b). North of Inuvik, the DH-ITH traverses the South Caribou Hills, which have a hummocky topography due to the variable thickness of unconsolidated deposits (Rampton, 1988). Topographic depressions are poorly drained and often host polygonal peatlands. Permafrost, on the order of 100-m thick near Inuvik, is continuous with temperatures ranging from -1 to -3 °C (Burn and Kokelj, 2009; Kokelj *et al.*, 2017b). Segregated ice is common in the upper 2-3 m of the ground and wedge ice is present in peatlands, with polygonal terrain increasingly common northward in association with lower snow and colder ground temperatures (Heginbottom *et al.*, 1995; Kokelj *et al.*, 2014; O'Neill *et al.*, 2019). The vegetation transitions from open spruce forest around Inuvik to tall shrub tundra in the north (Lantz *et al.*, 2013; Kokelj *et al.*, 2017b).

3.3 Arctic Coastal Plain

3.3.1 Mackenzie Delta (DH 725 to 737 km, ITH 0 to 12 km)

The DH-ITH alignment does not traverse the Mackenzie Delta physiographic division, however, the edge of the 10-km wide study corridor does (Figure 1). The Mackenzie Delta is a modern or Holocene delta comprised of alluvial materials typically greater than 50 m in thickness (Rampton, 1988). The north-northwest-trending elongated alluvial plain gently slopes from 10 m asl at its apex to sea level at the coast (Rampton, 1988). The delta is occupied by thousands of small ponds and lakes and stream channels of varying size and depth. Permafrost is continuous in terrestrial surfaces with thickness ranging from 74 to 90 m in the outer delta and 80 m near Inuvik (Johnston and Brown, 1965; Burgess *et al.*, 1982; Burn and Kokelj, 2009). Thermokarst lakes are common in the upper part of the delta where the permafrost is thick and through-going taliks are common under most of the lakes. Permafrost temperatures range from -1.5 to -3 °C in the upper delta and -3 to -5 °C in the outer delta (Burn and Kokelj, 2009, Fig. 11). Ground ice is present as pore ice, wedge ice, though predominantly as aggradational ice in the upper 2-4 m of the ground (Kokelj and Burn, 2004; 2005). Tree cover declines northward from open-spruce woodlands and peat plateaus transitioning, between 68.5°N to 69.5°N, to tall shrub tundra and then to sedge and dwarf shrub tundra.

3.3.2 Tuktoyaktuk Coastlands (ITH 40 to 138 km)

The Tuktoyaktuk Coastlands are low-lying, generally less than 60 m asl, and covered with a myriad of ponds, lakes, and wetlands (Mackay, 1974b; Burn and Kokelj, 2009). The rolling and hummocky fine-grained and stony till is interspersed with lacustrine plains (Aylsworth *et al.*, 2000a; Duk-Rodkin and Lemmen, 2000). Polygonal terrain and organic soils are common in poorly-drained areas (Kokelj *et al.*, 2014; Steedman *et al.*, 2017). Ice-rich permafrost underlies the area, thickening northwards from 100 m to over 500 m (Judge *et al.*, 1987; Burn and Kokelj, 2009; Kokelj *et al.*, 2017b). Ground ice is present as massive tabular ice and wedge ice, with segregated ice common in the upper 2 m of permafrost (Mackay, 1974b; Burn and Kokelj, 2009; Kokelj *et al.*, 2014). Retrogressive thaw slumping, indicative of ice-rich sediments, is common along lakeshores (Kokelj *et al.* 2009). Ground temperatures in undisturbed upland surfaces range from -5 °C to -7 °C where snow pack is thin (Burn and Kokelj, 2009). However, riparian areas with tall shrubs or slopes that accumulate snow can be associated with warmer permafrost or surface taliks (Kokelj *et al.*, 2017b). The vegetation is predominately dwarf shrub tundra (Lantz *et al.*, 2013).

4 CLASSIFICATION SCHEME

Features are digitized and classified according to their primary formational process: mass movement, periglacial, and hydrological (Table 2). The features are then further classed according to type, subtype, and subtype description. For cases where the subtype or subtype description is not relevant to the feature, the field is denoted as *not applicable*. In situations where a field attribute is undiscernible, it is labelled as *unclassified*.

Table 2. Feature classes, types, subtypes, and subtype description, where applicable.

Mass movement	Periglacial	Hydrological
Flow	Ice-wedge polygons	Beaded stream
Active-layer detachment	High-centre	Drained-lake basin
Debris flow / fan	Low-centre	Fully-drained
Retrogressive thaw slump	Undifferentiated	Partially-drained
Solifluction	String / net fen	Icing
Lobes	Palsa	Lake / pond affected by thermokarst
Terraces	Peat plateau complex	Oriented
Sheet (stripes)	Thermokarst mounds	Thermokarst gully
Rock glacier	Pingo	
Slide	Lithalsa	
Rotational slide		
Translational slide		
Shoreline slump		
Fall		
Rock fall		
Topple		
Block failure		
Complex		

4.1 Mass Movement Features

The main types of mass movement features are flows, slides, falls, topples, and complex failures. These types are subdivided into several different subtypes as discussed below. Mass movements can occur in soil or rock and are distinguished by their mechanism of failure, which can also be reflected in their morphology (Aylsworth *et al.*, 2000b). In addition to the information in Table 2, mass movements are classed as *active* (recent) and *inactive* (stabilized) features, if differentiable, and by the material in which the failure occurred, *bedrock* or *unconsolidated sediments*.

4.1.1 Flows

Flows exhibit a fluid character, showing evidence of movement throughout the failure (Aylsworth *et al.*, 2000b). The main flow-type failures are described below.

4.1.1.1 Active-layer Detachment

Active-layer detachments are shallow failures involving the downslope movement of only the active layer and the vegetation mat (Aylsworth *et al.*, 2000b). Movement may involve sliding of thawed soils over frozen ground, typically parallel to the surface, or manifest as a flow of water-saturated sediment known as a skin flow (Figure 3) (Harris *et al.*, 1988; Lewkowicz and Harris, 2005). They can develop on footslope, midslope, or crestslope segments or extend from slope crest to valley bottom on very gentle to moderate slopes but are most common on moderately to steeply incised valley sides (Figure 3). These features are often initiated after the active layer has been disturbed, such as in burn scars or in areas de-vegetated via avalanche activity, or as a result of increased precipitation or warm temperatures (Mollard and Janes, 1984; Aylsworth, *et al.*, 2000b). Several active-layer detachments may occur parallel to one another on the same hillslope, coalescing into a broad, sheet-like deposit at the bottom (Mollard and Janes, 1984). Gullied slopes are often the legacy of repeated sliding events.

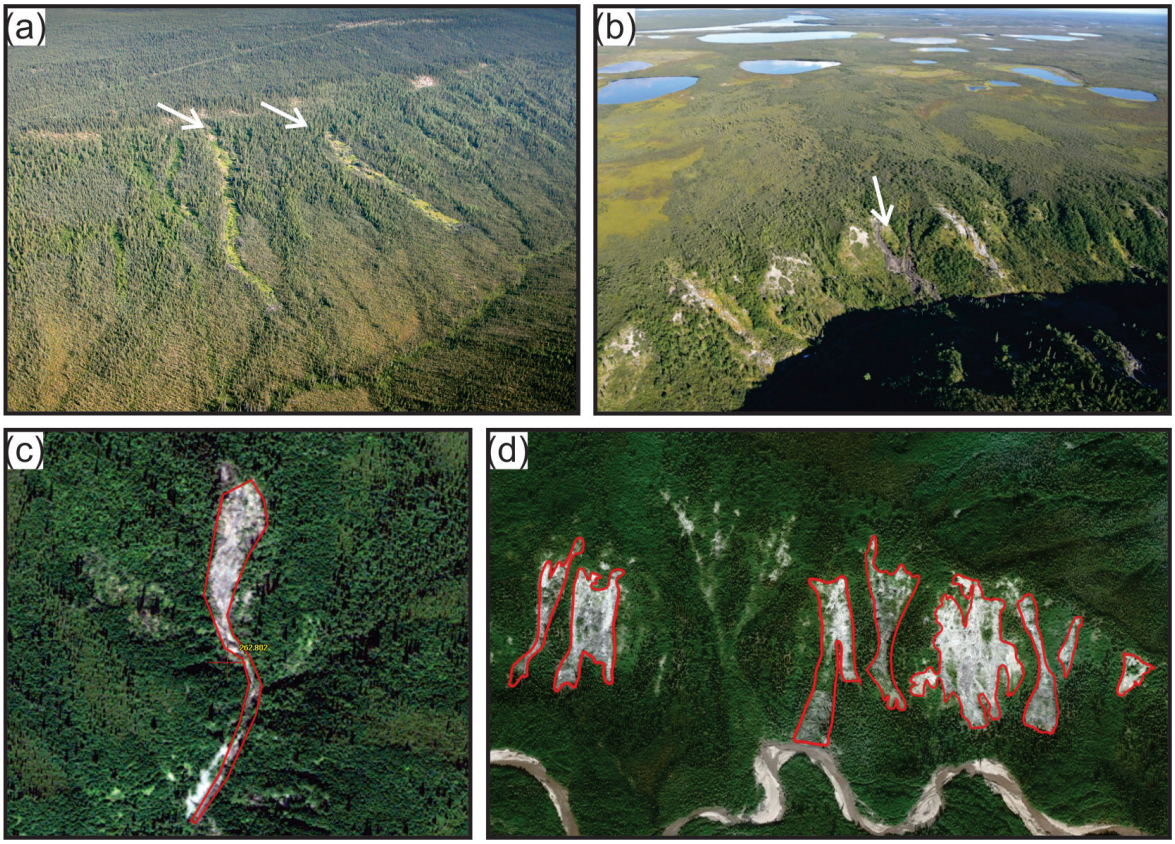

Figure 3. Active-layer detachment slides (ALD). (a) Re-vegetated, inactive ALDs (noted by arrows) on Eagle Plain (65.89°N, 127.42°W) (Modified from Huscroft *et al.*, 2019) (b) ALDs north of Inuvik (68.56°N, 133.83°W); arrow points to a recent ALD (Photograph by P.D. Morse. NRCan photo 2020-211). (c) and (d) Digitized active-layer detachments on the Peel Plateau at 67.20°N, 135.43°W and 67.19°N, 135.30°W, respectively.

4.1.1.2 Debris Flow / Fan

A debris flow is the rapid flow of water-saturated sediment that occurs in areas of high relief and high gradients (Figure 4) (Aylsworth *et al.*, 2000b). Debris flows are typically long and narrow, and widen into debris fans at their base. These flows commonly occur in mountainous terrain on established paths, usually steep gullies or drainage channels (Hungr *et al.*, 2014). Debris flows may be triggered by heavy rainfall, a slide, avalanche, rock fall, or deep thaw from unseasonally warm temperatures. Debris fans are fan-shaped deposits formed by the accumulation of debris flow material and ordinary fluvial bedload at the base of debris flow gullies or drainage channels (Figure 4) (Hungr *et al.*, 2014). Debris deposits, often referred to as "debris tongues", are commonly associated with mega retrogressive thaw slumps (Figure 5) (van der Sluijs *et al.*, 2018).

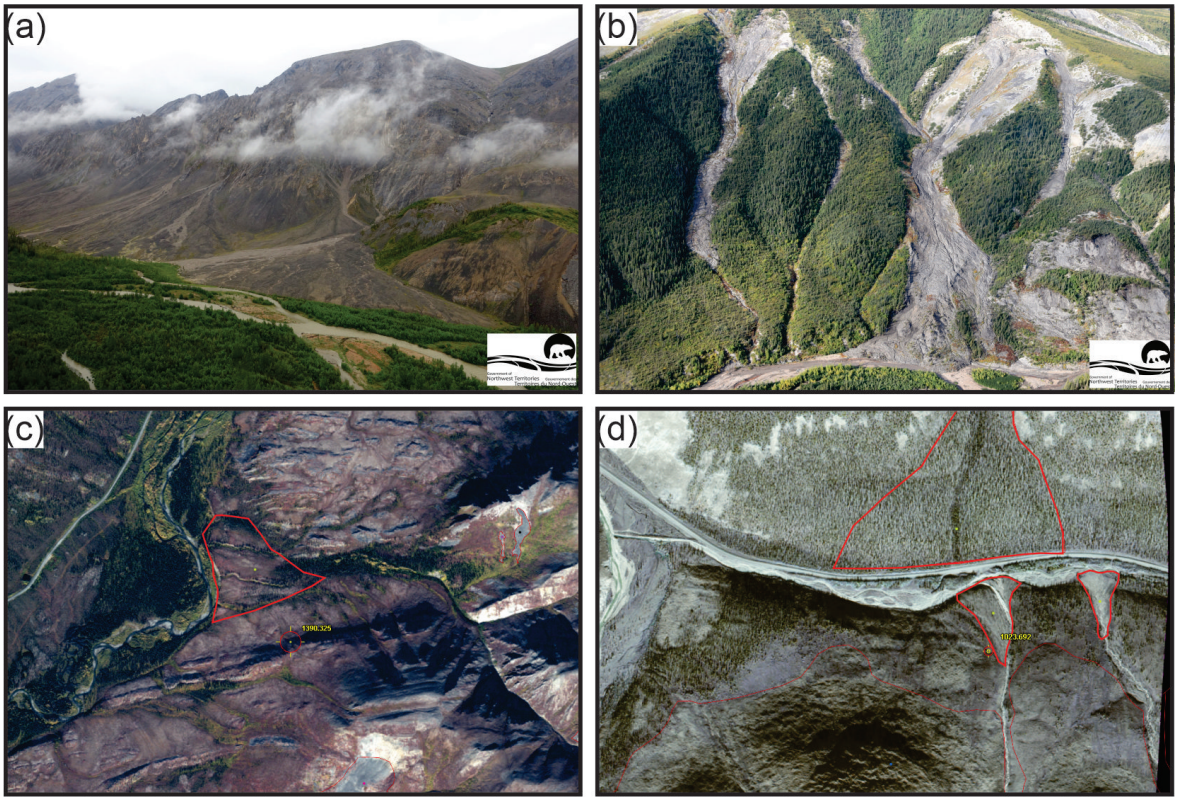

Figure 4. Debris flow / fan deposits (a) near Mountain River on the Mackenzie Plain (65.22°N, 128.47°W) and (b) near Willow River in the Richardson Mountains (67.85°N, 135.48°N) (photo (a) and (b) courtesy of NTGS). (c) and (d) Digitized debris fan deposits in the Ogilvie Mountains (64.42°N, 138.26°W and 65.07°N, 138.31°N, respectively).

4.1.1.3 Retrogressive Thaw Slump

Retrogressive thaw slumps occur in areas underlain by thick layers of excess ground ice (Kokelj *et al.*, 2017c). Thaw slumps can be initiated by a range of processes including fluvial erosion, wave action along shorelines, thermal degradation and subsidence, or shallow active-layer detachments which remove overburden and expose underlying ground ice. The headwall gradually erodes upslope as ice-rich permafrost ablates so that a slump can remain active and continue to enlarge for several decades (Lacelle *et al.*, 2015; van der Sluijs *et al.*, 2018). The accumulation of saturated materials at the base of the headwall can be transported downslope by a suite of processes ranging from rapid fluidized flows, to sliding, to slow creep depending on material properties, slope, and degree of saturation (Aylsworth *et al.*, 2000b; Kokelj *et al.*, 2009; 2015). As a result, the morphology of scar zone and debris tongue deposits may range from a series of ridges at the toe of the slope where sediment accumulates, to flow deposits comprising 10^4 to 10^6 m^3 of materials that can extend hundreds of metres into downstream environments (van der Sluijs *et al.*, 2018). Where thaw slumps occur along shorelines, debris deposits often enter into the adjacent water body and are not discernable from aerial imagery.

Thaw slumps are identified through the characteristic steep, bowl-shaped headwall and low-angle tongue or slump ridges (Figure 5) (Aylsworth *et al.*, 2000b). Retrogressive thaw slumps are deeper than active-layer detachments because they form as a result of thawing permafrost. Slumps typically occur in proximity to the failure mechanism that could expose ice, such as channel, lakeside, or coastal erosion or near the crest of a slope (Mollard and Janes, 1984). However, continued enlargement of features in association with climate warming has created mega-slumps where active headwalls tens of metres in height may grow hundreds of metres upslope from the point of initiation

(Kokelj *et al.*, 2015). If present, the debris tongue flowing out from the active scar area can raise the suspended sediment and solute loads in downstream lake and stream environments by several orders of magnitude (Kokelj *et al.*, 2005; 2013). Thaw slumps stabilize when materials accumulate and insulate the ice-rich headwall. Inactive thaw slumps, which are mapped as well, can be identified by upper edges that are less abrupt than in active features. Nutrient-rich soils in the scar zone accommodate rapid colonization of plant or shrub communities that are typically distinct from the adjacent forest or tundra (Lantz *et al.*, 2009).

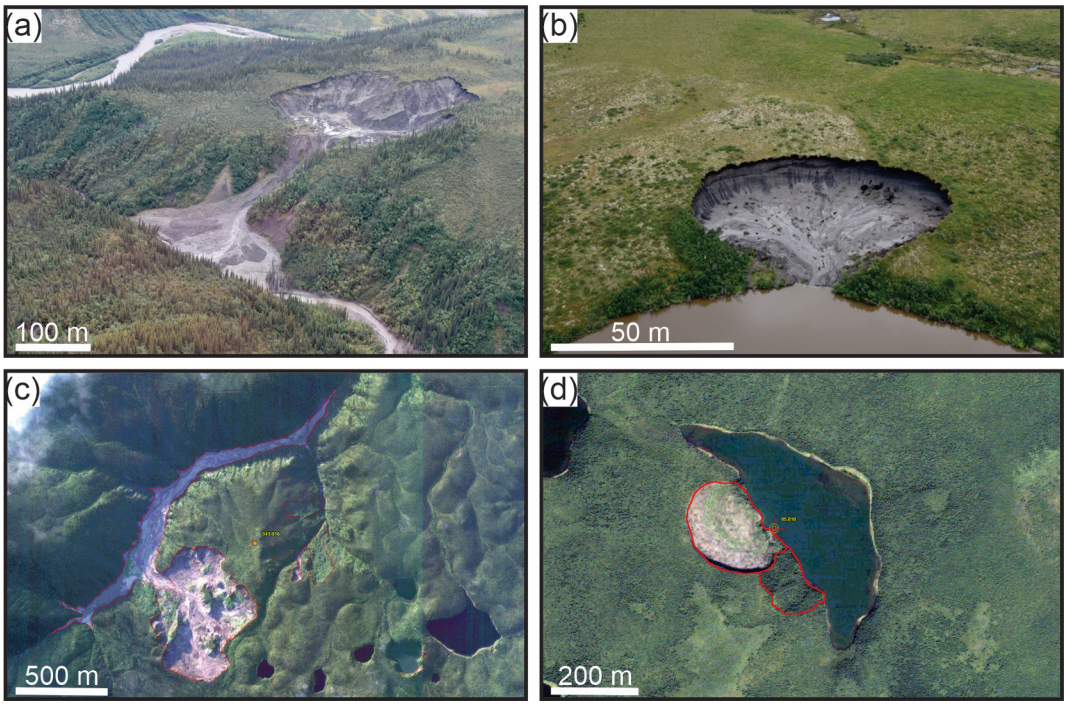

Figure 5. Retrogressive thaw slump (RTS) examples: (a) with a debris fan deposit in the Peel Plateau west of Fort McPherson (67.36°N, 135.30°W) (Photograph by P.D. Morse. NRCan photo 2020-212), and (b) adjacent to a lake north of Inuvik in the Anderson Plain (68.59°N, 133.51°W) (Photograph by P.D. Morse. NRCan photo 2020-213). (c) Digitized mega RTS with a debris tongue in the Peel Plateau (67.26°N, 135.22°W), smaller active and inactive RTSs are visible to the right of the mega RTS; and (d) in the Anderson Plain, north of Inuvik where an active RTS and inactive RTS are shown (68.53°N, 133.74°W).

4.1.1.4 Solifluction

Solifluction is the downslope movement of unconsolidated material by frost creep and gelifluction (French, 2007). Frost creep is the ratchet-like downslope movement of soil particles from frost heaving (typically normal to the slope) and subsequent thaw settlement (typically vertical) (Washburn, 1980). Gelifluction is the flow component of solifluction characterized by the slow downslope movement of saturated soil particles generally limited to the upper 50 cm of the active layer (French, 2007). Movement rates range from 0.02 to 12.0 cm yr^{-1} (French, 2007, Table 9.1, p. 226). Areas with tundra or little vegetation are more susceptible to solifluction (Mollard and Janes, 1984; French, 2007). Larger clasts tend to have their long axis oriented parallel to slope. Solifluction can manifest as broad sheets with lobate fronts, isolated tongue-shaped lobes, stripes, and bench-like terraces (Harris *et al.*, 1988) (Figure 6).

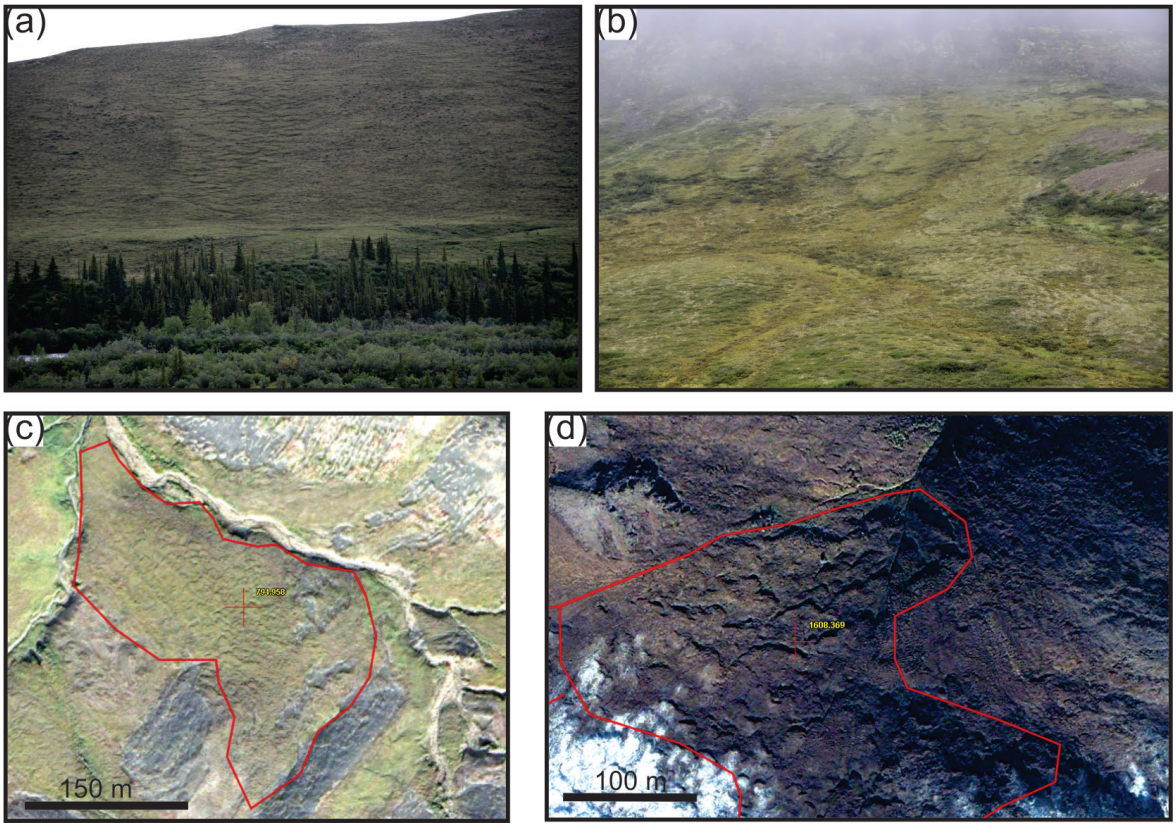

Figure 6. Examples of solifluction lobes along the Dempster Highway. (a) Ogilvie Mountains (64.87°N, 138.29°W) and (b) Richardson Mountains (67.18°N, 135.78°W) (Photographs by P.D. Morse. NRCan photos 2020-214 (a) and 2020-215 (b)). Solifluction lobes digitized in Summit in (c) the Richardson Mountains (67.20°N, 135.85°W) and (d) the Ogilvie Mountains (64.65°N, 138.45°W). In both (c) and (d), movement downslope is towards the top right of the image.

4.1.1.5 Rock Glacier

A rock glacier is a tongue-shaped or lobate body of frozen debris with interstitial ice and ice lenses that moves downslope or down-valley by deformation of the ice within it (Figure 7) (French, 2007). Rock glaciers are periglacial features found in steep, mountainous terrain, where there is an adequate supply of debris. Rock glaciers, found below talus slopes, typically derive their debris from the adjacent talus slopes, where as the debris source for rock glaciers found below glaciers is commonly from the adjacent moraines. The rock glacier surface is characterized by ridges and furrows that are often arcuate and convex downslope but may also be longitudinal (Washburn, 1980). An active rock glacier has a steep front, greater than the angle of repose (Harris *et al.*, 1988). The surface texture of the rock glacier commonly differs from the texture of the surrounding slopes (Stumm *et al.*, 2015).

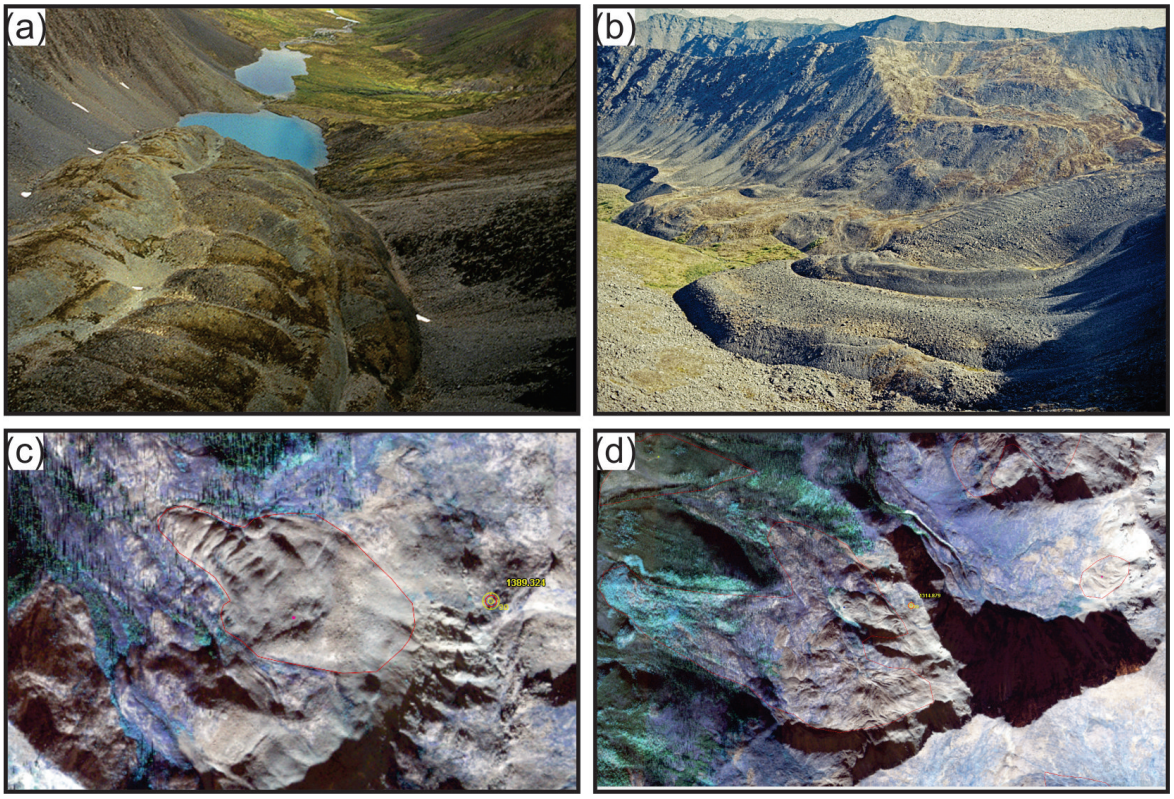

Figure 7. Examples of rock glaciers in the southern Ogilvie Mountains. (a) and (b) Oblique photos showing characteristic ridges and furrows on surface (Modified from Huscroft *et al.*, 2019). Digitized rock glaciers in Summit (c) (64.33°N, 138.38°W) and (d) (64.28°N, 138.43°W).

4.1.2 Slides

Slides, in comparison to flows, show more rigid movement where slide debris consists of more or less intact blocks (Figure 8). The main slide-type mass movements are described below.

4.1.2.1 Rotational Slide

Rotational slides involve the downslope movement of a rigid block of sediment or rock along a curved failure plane (Figure 8a) (Aylsworth *et al.*, 2000b; Dyke, 2000). These soil or rock slumps typically exhibit a prominent head scarp and a back-tilted bench forming the top of the slide. In some cases, there may be a series of blocks and the toe of the slide may extend beyond the original slope. The slide body typically shows little internal deformation. They are often triggered by stream erosion, extreme rainfall, and removal of vegetation by logging or fire (Dyke, 2000; Hungr *et al.*, 2014).

4.1.2.2 Translational Slide

Translational slides involve the sliding of a block of cohesive soil or rock on an inclined planar weak layer, which is often pre-sheared, a bedrock bedding plane, or a discontinuity (Figure 8b) (Aylsworth *et al.*, 2000b). These slides may be triggered by fluvial erosion at the base of an inclined bedding plane. The slide mass separates from the stable soil or rock along a deep tension crack at the head. The surface may appear stepped forward with little to no internal deformation of the slide mass. A vertical tension crack may be present between the head scarp and the slide mass. Planar slides are common in layered, folded sedimentary rocks, schistosity or fault planes in metamorphic rocks, and relief joints in intrusive rocks (Hungr *et al.*, 2014) and mountainous areas (Aylsworth *et al.*, 2000b).

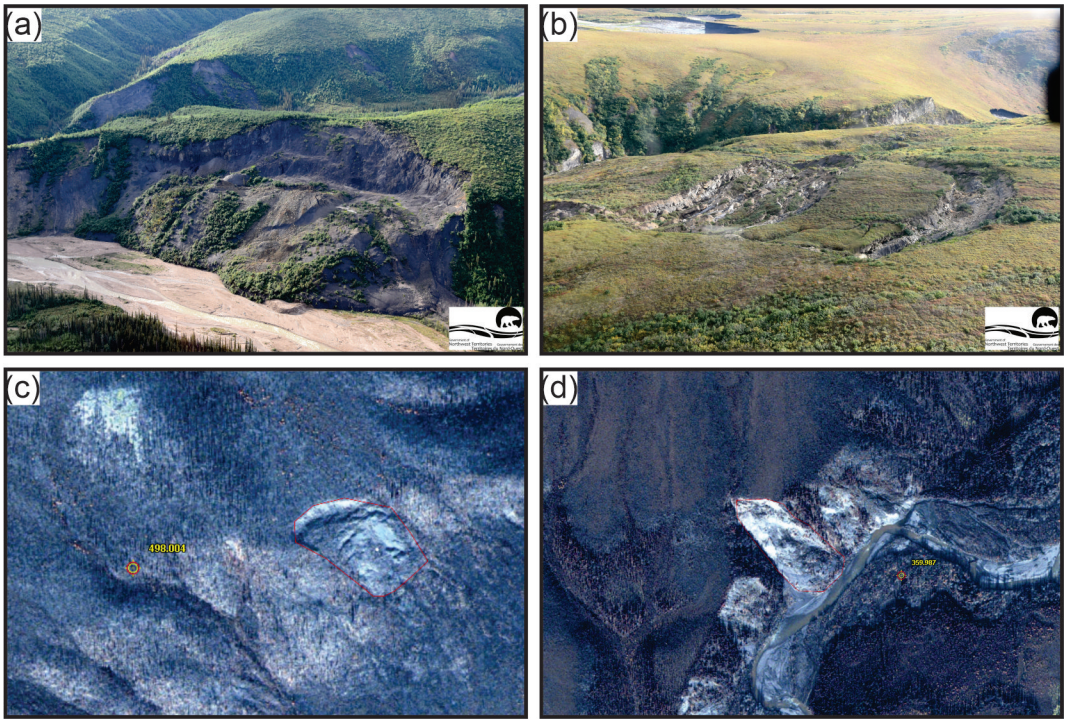

Figure 8. (a) Rotational slide on Little Bear River in the Mackenzie Mountains (64.48°N, 126.46°W) (photo courtesy of NTGS). (b) Translational slide near Willow River in the Richardson Mountains (68.07°N, 135.68°W) (photo courtesy of NTGS). Deep-seated slides in the Eagle Plain: (c) Slide with the failure plane likely in unconsolidated quaternary sediments (66.41°N, 136.56°W); (d) Slide with the failure plane likely in bedrock (66.44°N, 136.53°W).

4.1.2.3 Shoreline Slump

Shoreline slumps represent a continuum between retrogressive thaw slumping and solifluction. These features are characterized by extended sections of over-steepened shoreline with a head scarp typically running parallel to the shore (Figure 9). The features result where retrogressive thaw of underlying permafrost has destabilized slope materials accelerating downslope movement. This perturbation commonly stimulates colonization by tall shrubs which often characterize these features. The disturbance develops when wave action, or warming and lateral migration of the frozen-unfrozen interface subjacent to the shoreline destabilizes the toe of the slope and initiates a failure sequence that retrogresses upslope. If this process exposes excess ice then a retrogressive thaw slump may develop.

Figure 9. Shoreline slumping on the southwest shore of Eskimo Lakes in the Tuktoyaktuk Coastlands (68.88°N, 133.29°W) (Photograph by P.D. Morse. NRCan photo 2020-216).

4.1.3 Falls and Topples

Topples involve the forward rotation of a mass due to gravity; whereas falls are the detachment of soil or rock from a steep slope that moves downslope by falling, bouncing, or rolling (Cruden and Varnes, 1996).

4.1.3.1 Rock Fall

A rock fall is the detachment, fall, rolling, and bouncing of rock fragments downslope (Hungr *et al.*, 2014), where the rock fragments interact more with their path than each other. Events tend to be episodic and deposits are limited in extent. Falls may be caused by freeze-thaw action in joints and faults. These features are restricted primarily to mountainous regions or areas with steep rock slopes (French, 2007). Talus commonly accumulates at the base of the rock face and is of limited volume (French, 2007; Hungr *et al.*, 2014).

4.1.3.2 Block Failure

Block failures are topples that are commonly found along river and coastal banks in permafrost regions (Lawson, 1983). They consist of large overturned or slumped blocks of intact sediment, commonly cemented by ice (Figure 10). Undercutting by thermal erosional niching causes failure. If present, ice wedges control the initial size and geometry of the blocks as failure preferentially occurs along the face of the wedges (Walker and Arnborg, 1963). Block failures are common in semi-cohesive, fine-grained sediments (Lawson, 1983).

Figure 10. Oblique aerial view of block failures on the west shore of Eskimo Lakes (68.98°N, 133.23°W) (Photograph by P.D. Morse. NRCan photo 2020-217). Note the overturned vegetated block of sediment and ice-wedge polygon network adjacent to the shore.

4.1.4 Complex Mass Movements

Complex mass movements refer to mass movements that exhibit more than one type of failure mechanism. An example of this is a retrogressive failure that has evolved to produce a debris flow tongue (Figure 5). In warmer discontinuous permafrost, deep-seated slides often evolve into retrogressive features, particularly where ice-rich materials are present (Figure 11). The evolution of features over time can influence their identification requiring a polymorphic terminology identified as complex in this case.

Figure 11. Complex mass movement involving a deep-seated rotational slide (centre) that triggered a retrogressive thaw slump above, which in turn produced a debris flow tongue (foreground), Willow River in the Richardson Mountains (68.11°N, 135.62°W) (photo courtesy of NTGS).

4.2 Periglacial Features

4.2.1 Ice-wedge Polygons

Ice-wedge polygons are the geometric surface expression of an underlying ice-wedge network (Figure 12) (Lachenbruch, 1962). The polygonal shapes are delimited by troughs, which are underlain by wedge ice and are typically bounded by a ridge on either side. Ice wedges form by thermal contraction cracking of the ground in winter and infilling by snowmelt, which freezes to form a vein of ice, increasing the size of the wedge (Mackay, 1974a; 1993). *High-centred polygons* typically lack the ridges that bound the troughs of *low-centred polygons*. The latter also typically develop in flat areas and may have water ponded in the polygon centres (Mollard and Janes, 1984). Ice wedges commonly develop in organic deposits, glacial tills, or fluvial outwash plains (Mollard and Janes, 1984; Gray and Seppälä, 1991). Ice-wedge networks and polygonal terrain commonly develop over extensive areas that share similar soil type, drainage, and thermal conditions and are easy to identify. Polygons are most prominent on the tundra where colder ground temperatures promote thermal contraction cracking and ice wedge growth (Kokelj *et al.*, 2014). However, polygons also occur in boreal peatlands and forested areas where patterns of spruce cover can reveal presence of ice-wedge networks (Kokelj and Burn, 2004). It is common for a low-centred polygon to contain a pool of water in the centre, if a few polygons exhibit ponding it may be assumed that the surrounding polygons are also low centred. In larger fields, low-centred polygons may transition to high-centred features with subtle changes in drainage and topography. In high-centred polygon fields, ponding is typically limited to trough depressions. Ice-wedge polygons that are not discernible as high- or low-centred are classified as *undifferentiated*.

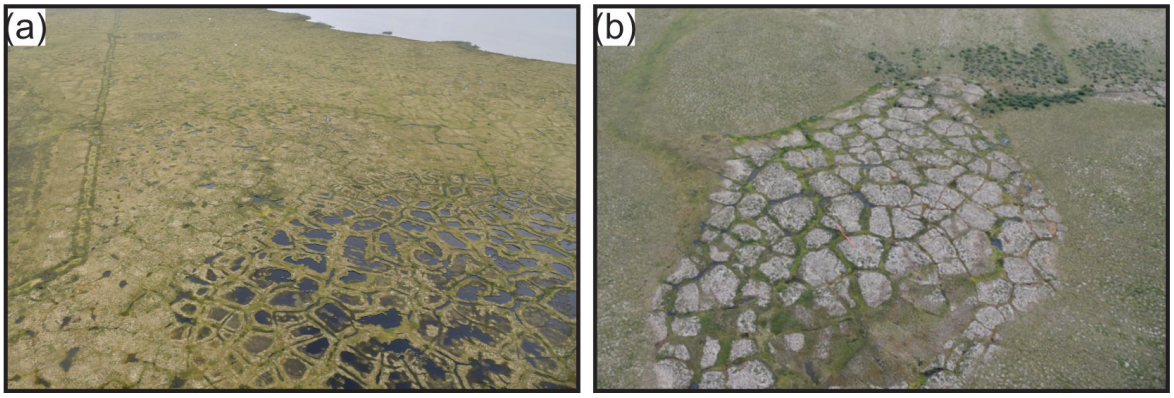

Figure 12. (a) Low-centre ice-wedge polygons (69.27°N, 133.11°W), note the ponding in the centre of the polygons (Photograph by P.D. Morse. NRCan photo 2020-218). (b) High-centre ice-wedge polygons southwest of Eskimo Lakes (68.76°N, 133.55°W) (Photograph by P.D. Morse. NRCan photo 2020-219).

4.2.2 String / Net Fen

A string fen, also called a ribbed fen, consists of a series of narrow (1-3 m) peat ridges, called strings, which are interspersed with slight depressions that may contain shallow pools (Figure 13) (Warner and Rubec, 1997; Woo, 2012). The depressions are dominated by fenland vegetation (sedges and mosses) while the better-drained ridges support shrub and tree vegetation (Zoltai and Tarnocai, 1975). The ridges can reach up to 1 m in height and several hundred metres in length and are typically underlain by permafrost in areas of perennially frozen terrain (Zoltai and Tarnocai, 1975; Woo, 2012). The ridges in string fens form subparallel lines perpendicular to surface flow, while the ridges in net fens have a reticulate, irregular net-like pattern (Warner and Rubec, 1997; Woo, 2012).

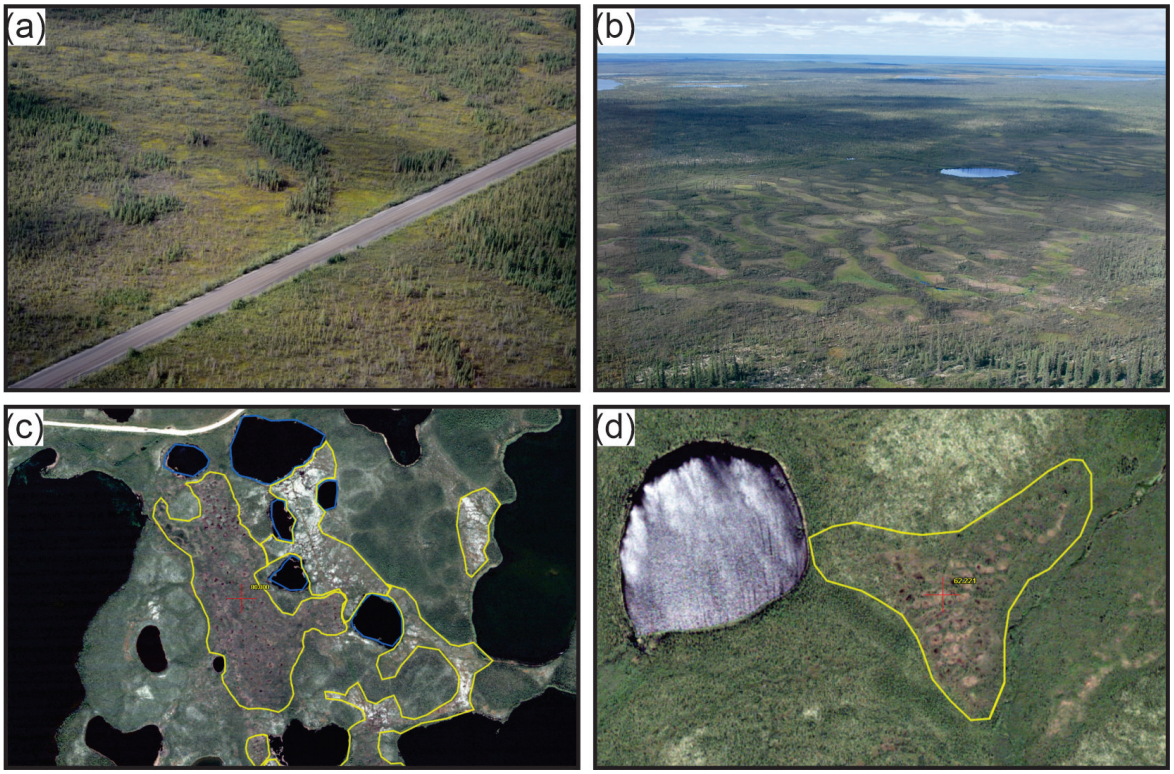

Figure 13. (a) String fen is visible in the top half of the image, near the Dempster Highway, north of Tsiigehtchic (67.67°N, 133.84°W) (Photograph by P.D. Morse. NRCan photo 2020-220). (b) String fen near Inuvik (photo courtesy of A. Branson). (c) Digitized fen and peat plateau terrain west of Tsiigehtchic (67.41°N, 133.92°W). (d) Digitized net fen southwest of Tsiigehtchic (67.36°N, 134.02°W).

4.2.3 Palsa

A palsa is a peaty permafrost mound with a core of alternating layers of segregated ice and peat or mineral soil material (Harris *et al.*, 1988). Typically, palsas are circular or oval; 2 to 100 m in diameter; and vary between 1 and 7 m in height. Palsas are most commonly found in discontinuous permafrost in association with wet peatlands (Figure 14). Palsas may occur individually or in clusters (Williams and Smith, 1989; Coultish and Lewkowicz, 2003; French, 2007). Palsa initiation is likely due to thin snow cover (Seppälä, 1982; Williams and Smith, 1989), or modification of local drainage conditions (Coultish and Lewkowicz, 2003). Their elevated surface promotes a thin snow cover enhancing winter cooling while the peat surface will dry out in summer and provide thermal insulation. The mineral soil beneath a palsa is commonly fine-grained (Zoltai and Tarnocai, 1975).

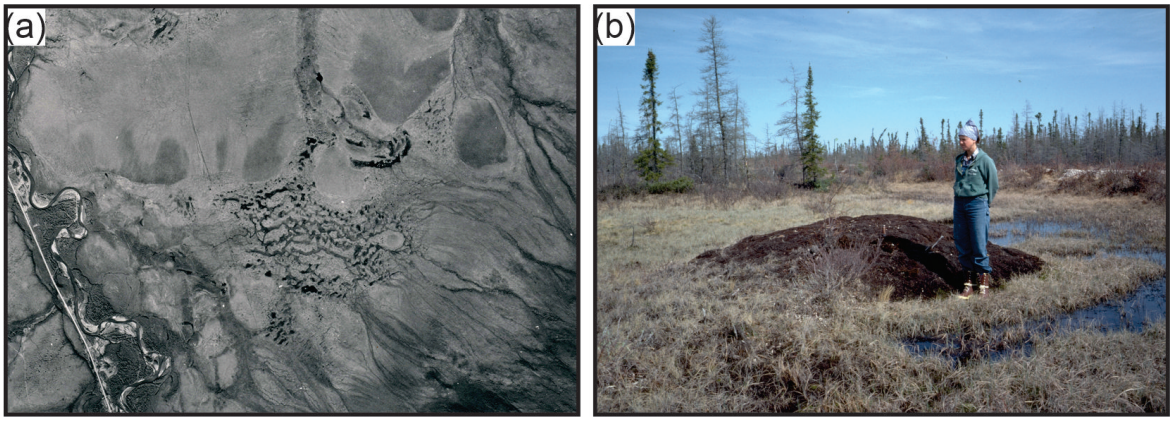

Figure 14. (a) Palsas located within fens along the Dempster highway near km 88 in the Ogilvie Mountains (64.68°N, 138.36°W; photo credit: NAPL A18137; modified from Huscroft *et al.*, 2019). (b) Palsa (image centre) located within a fen near Faro, Yukon (Photograph by L. Dredge. NRCan photo 2001-155).

4.2.4 Peat Plateau Complex

Peat plateaus are elevated, flat-topped peatlands that have a perennially frozen core and are often surrounded by fen (Figure 15) (Zoltai, 1972). The elevation of peat plateaus results from freezing of the peat and formation of segregated ice lenses, which may penetrate the underlying mineral soil. Although similar to palsas, peat plateaus tend to have an irregular shape; be more extensive, reaching several kilometres; and lower in height, seldom exceeding 1.2 m (Zoltai, 1972; French, 2007). Peat plateaus are common in discontinuous permafrost. Polygonal peat plateaus resemble a peat plateau but the surface is dissected by troughs, rectangular drainage patterns, and sometimes ponds that typically delineate high-centred polygons, together indicating the presence of an underlying ice-wedge network (Zoltai and Tarnocai, 1975). In areas of warm and thin permafrost, peat plateaus are distinguished from collapsed scar areas, which can coalesce to form collapse basins and wetland areas often exhibiting characteristics of a string bog. Collapse of peat plateaus is rapidly increasing in extent due to climate-driven thawing or forest fire (Gibson *et al.*, 2018).

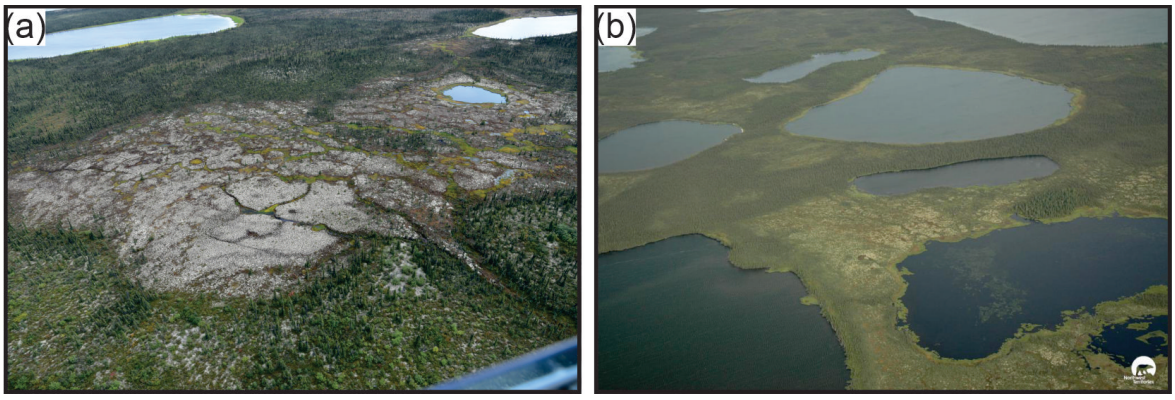

Figure 15. Lichen-covered peat plateaus near Tsiigehtchic. (a) Peat plateau (light-coloured) and fen (bright green) complex on the Anderson Plain (67.44°N, 133.29°W) (Photograph by P.D. Morse. NRCan photo 2020-221). (b) Peat plateau complexes on the Peel Plain (67.40°N, 133.95°W) (modified from NWT Centre for Geomatics, 2020).

4.2.5 Thermokarst Mounds

A "badland-like" relief can develop as a result of top-down ice wedge thaw and/or erosion operating preferentially along troughs overlying ice wedges in unconsolidated sediment (Harris *et al.*, 1988; French, 2007) (Figure 16). Preferential fluvial erosion along ice wedges may lead to isolated conical thermokarst *mounds* (*baydzherakh* in Russian) (Godin and Fortier, 2012). Thermokarst mounds mainly occur in groups forming a distinctive surficial network of regularly shaped mounds separated by troughs formed by melted ice wedges (Harris *et al.*, 1988), and which may be found adjacent to ice-wedge polygon networks (French, 2007).

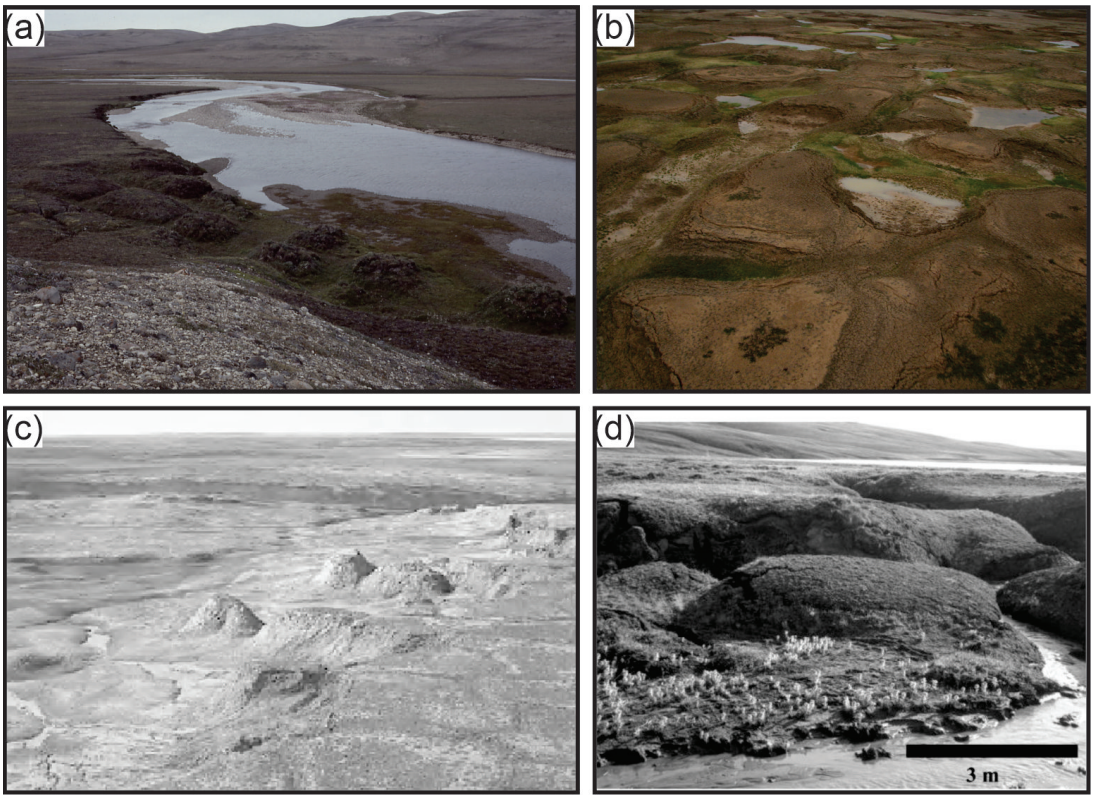

Figure 16. (a) View of thermokarst mounds near Sachs River on southern Banks Island; note original ice-wedge network to the left of the mounds (photo courtesy of A.G. Lewkowicz). (b) View of thermokarst mounds on northern Banks Island (photo courtesy of A.G. Lewkowicz). (c) Oblique view of badland-like relief on eastern Banks Island, note remnants of the original ice-wedge polygon surface in the foreground of image (modified from French, 2007). (d) Thermokarst mounds on Bylot Island in Nunavut (modified from Godin and Fortier, 2012).

4.2.6 Pingo

A pingo is a perennially-frozen mound, typically conical in shape, covered with soil and vegetation and consisting of a core of massive ice (Harris *et al.*, 1988). Pingos occur in continuous and discontinuous permafrost areas. These mounds may vary in height from a few metres to over 60 m and up to 300 m in diameter (French, 2007). Typically, pingos are conical, somewhat asymmetric, with a circular or oval base (Figure 17). The top may be fissured by dilation cracks that result from rupturing of the soil and vegetation cover due to progressive heave caused by development of the ice core (Hughes, 1969; Harris *et al.*, 1988). There are two types of pingos, open-system and closed-system, based on their growth mechanism.

Open-system pingos, also known as hydraulic pingos, develop from the freezing of injected water supplied by intra- or subpermafrost groundwater that flows downslope, under a hydraulic gradient (Mackay, 1998). As a result, open-system pingos are mainly located in discontinuous permafrost in association with areas of prominent topographic relief (Harris *et al.*, 1988), and commonly occur in isolation or in small groups in areas such as hillslopes, alluvial fans, and valley bottoms (French, 2007). In interior Yukon, open-system pingos are found to be most abundant in unglaciated, narrow valleys and old glaciated terrain (Hughes, 1969). Typically, they occur at the break in slope, between the valley floor and wall, of east- and southeast-facing slopes (Hughes, 1969).

Closed-system pingos, also known as hydrostatic pingos, result from pore-water expulsion caused by aggrading permafrost beneath drained-lake surfaces that are underlain by saturated sands (Mackay, 1998). Therefore, closed-system or hydrostatic pingos are often found in shallow lakes or former lake basins where permafrost aggradation has occurred in previously unfrozen saturated sediment (French, 2007). They typically occur singly and not in groups. A high concentration of closed-system pingos are found on the Tuktoyaktuk Peninsula, because drainage caused by coastal erosion or permafrost thaw is common, and the lakes are underlain by sandy sediments (Mackay, 1992). Closed-system pingos may also form from freezing of localized taliks that formed beneath abandoned river channels (Pissart and French, 1976).

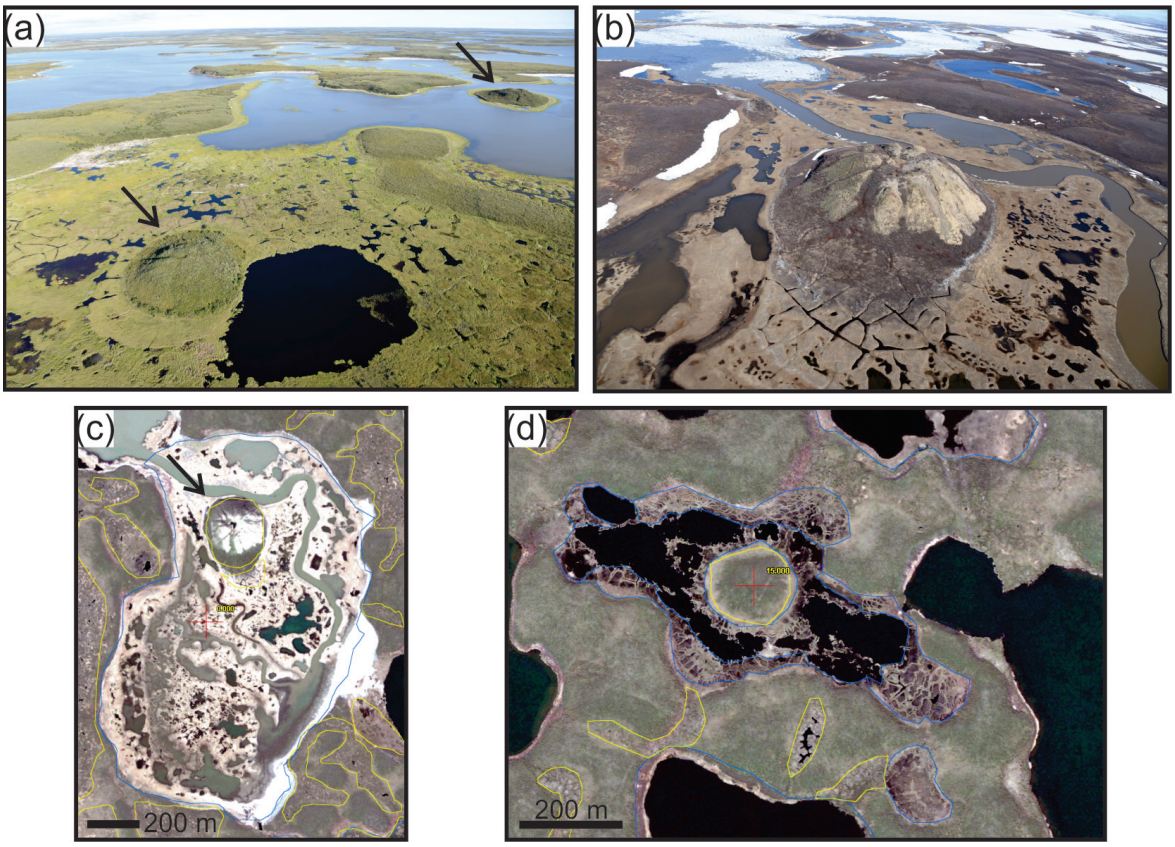

Figure 17. Images of closed-system pingos along the study corridor near Tuktoyaktuk. (a) Oblique air photo of two pingos in a former drained-lake basin partially inundated by the Beaufort Sea (69.38°N, 133.26°W) (Photograph by P.D. Morse. NRCan photo 2020-223). (b) Oblique photo of pingo in a drained-lake basin, note the polygonal pattern highlighted by ponding in the troughs and centres of the features adjacent to the pingo (69.40°N, 133.08°W) (Photograph by P.D. Morse. NRCan photo 2020-224). (c) Digitized pingo in (b) shown in Summit. Extent of drained-lake basin is visible. (d) Pingo in drained-lake basin with degraded ice wedges affected by thermokarst (69.37°N, 132.97°W).

4.2.7 Lithalsa

Lithalsas are permafrost mounds formed in mineral soils by ice segregation that occurs when permafrost aggrades into saturated fine-grained sediments (Harris, 1993). These ice-rich permafrost features are similar to palsas but lack a peaty stratigraphy and thick surface cover of peat (Pissart, 2002). The conditions favourable for lithalsa development include warm (0 to -1 °C MAGT) discontinuous permafrost, fine-grained frost-susceptible sediment, and an available groundwater supply (Wolfe *et al.*, 2014). Gradual aggradation of permafrost into saturated fine-grained frost-susceptible substrate inhibits rapid frost penetration and supports segregated ice lens formation and growth. Saturated sediment at depth supplies the water to the growing ice lenses (Gaanderse *et al.*, 2018), and the availability of the water supply likely affects the size, shape, and cryostratigraphy of the lithalsas. Lithalsas are found near water sources, such as within stream valleys, along shorelines, large lake basins, or adjacent to ponds (Figure 18). Their irregular shape and size are typically related to the pattern of permafrost aggradation, thickness of frost susceptible sediments, and distribution of the water source. Lithalsas form a distinct landscape feature because the well-drained mounds comprised of mineral soils are typically colonized by white spruce (*Picea mariana*) and birch (*Betula papyrifera*), and the topographically distinct features occur in conjunction with irregularly shaped lakes and ponds that show evidence of past thermokarst collapse.

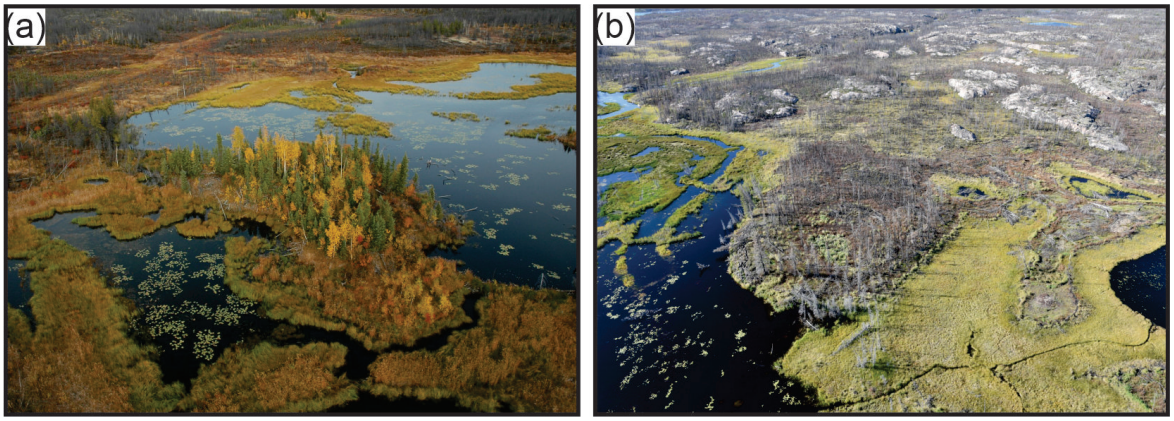

Figure 18. (a) Treed lithalsa near Lucky Lake, southwest of Discovery Mine, north of Yellowknife (63.14°N, 113.98°W) (Photograph by C. Duchesne. NRCan photo 2020-235). (b) Burned lithalsa adjacent to stream northwest of Yellowknife (62.63°N, 144.76°W) (Photograph by P.D. Morse. NRCan photo 2020-225).

4.3 Hydrological Features

4.3.1 Beaded Stream

A beaded stream is characterized by a series of small lakes or ponds connected by narrow reaches (Harris *et al.*, 1988; French, 2007). Thermal erosion of ground ice by the original stream creates depressions that fill with water resulting in a string of thermokarst ponds connected by a mutual drainage system (Figure 19). Beaded streams are common in permafrost regions and are often associated with riparian areas hosting ice-wedge polygon networks, which channelize drainage, promoting accelerated thermal erosion at the intersection of the ice-wedge polygons where ponds typically form (French, 2007).

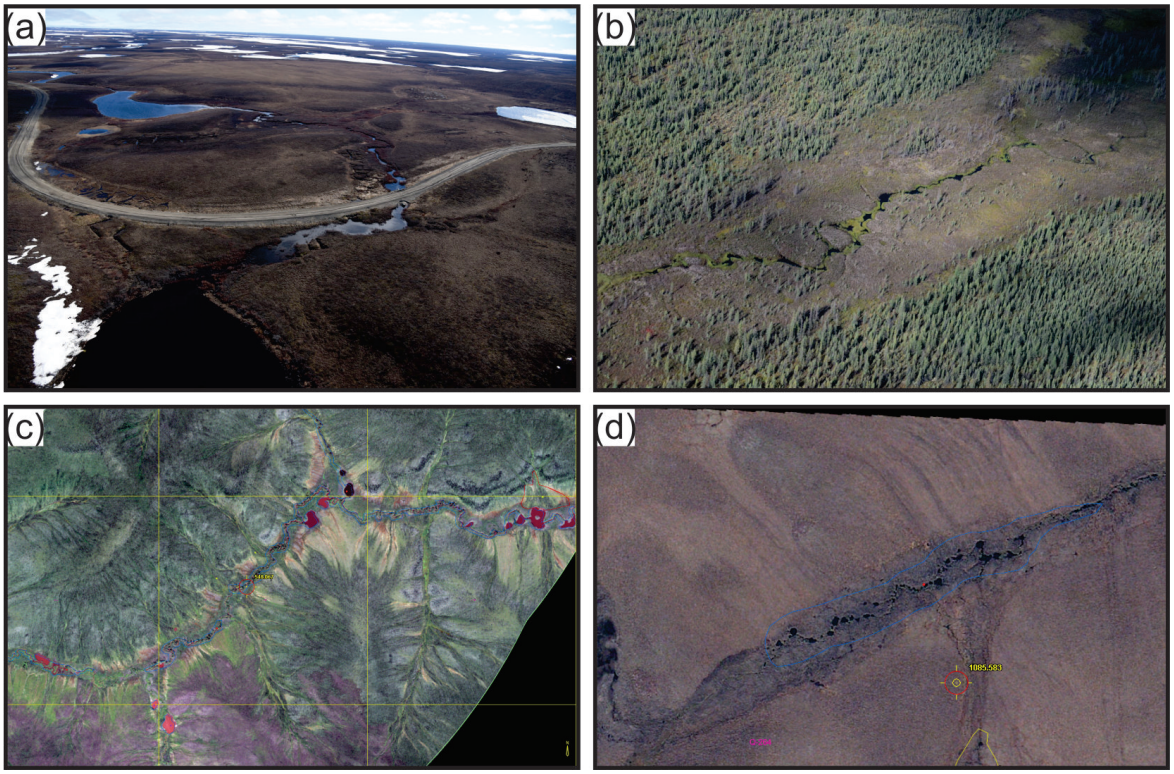

Figure 19. Beaded stream examples. (a) Beaded stream traversed by the ITH south of Tuktoyaktuk (69.34°N, 133.05°W) (Photograph by P.D. Morse. NRCan photo 2020-226). (b) Near the Dempster Highway between Tsiigehtchic and Inuvik (67.75°N, 133.81°W) (Photograph by P.D. Morse. NRCan photo 2020-227). (c) In the Eagle Plain (66.11°N, 137.18°W). (d) Ogilvie Mountains (64.75°N, 138.39°W).

4.3.2 Drained-lake Basin

A drained-lake basin develops when a lake has drained as a result of water that flowed through interconnected ice-wedge cracks or troughs of an ice-wedge polygon, overtopping of a snow dam, or along seepage channels, or has been truncated by coastal erosion or migration of an adjacent fluvial system (Figure 20) (Mackay, 1988). Drainage commonly occurs rapidly resulting in full or partial drainage, later characterized by residual ponds (Marsh *et al.*, 2009).

Drained lakes may be identified by well-defined abandoned shorelines, wetland vegetation that contrasts to the surrounding vegetation, or non-vegetated lacustrine sediments found on "recently" formed drained-lake basins, and an eroded outlet or drainage channel (Mackay, 1988; Marsh *et al.*, 2009). Pingos are common in drained-lake basins (Mackay, 1998; Figure 17). Drained-lake basins may be clustered in groups of connected lakes as drainage can trigger upstream or downstream drainage events (Mackay, 1988). Patterns of revegetation in recently drained lakes vary with substrate, climate, and moisture conditions within the basin. Over the long-term, these flattish, poorly-drained areas are typically locations of organic accumulation and peatland development. Throughout the study region, organic deposits hosting wedge ice and polygonal terrain commonly develop in drained-lake basins (Kokelj *et al.*, 2014).

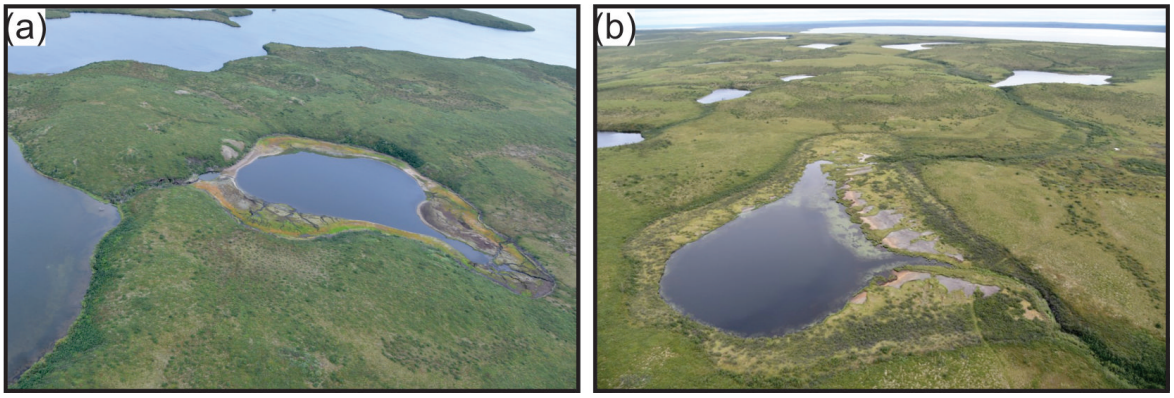

Figure 20. (a) Drained-lake basin with a residual pond south of Tuktoyaktuk (69.09°N, 133.22°W) (Photograph by P.D. Morse. NRCan photo 2020-228). Note the former shoreline and drainage channel to the left of the partially drained-lake basin. (b) Drained-lake basin with residual pond north of Noell Lake (68.59°N, 133.56°W) (Photograph by P.D. Morse. NRCan photo 2020-229). Note former shoreline and drainage channel at lower right of image. Shrub vegetation has colonized the former lake bottom.

4.3.3 Icing

An icing is a sheet-like mass of layered ice formed by the freezing of successive overflows of water that may seep from the ground, flow from a spring, or emerge from below river ice (Harris *et al.*, 1988). Icings commonly form in river valleys (Hu and Pollard, 1997; Crites *et al.*, 2020) and at the base of hillslopes (Yoshikawa *et al.*, 2007), but may also occur in flatter terrain (Morse and Wolfe, 2015).

Remnant ice observed in spring and summer imagery after the snow has melted is commonly an icing (Morse and Wolfe, 2015), especially if located in a river valley or at the base of a hillslope. A widening of braided channels is often associated with icing occurrences in gravel bed streams (Figure 21). Areas clear of vegetation in river valleys may be indicative of icing locations because the persistence of the ice cover into the growing season negatively affects the growth of vegetation.

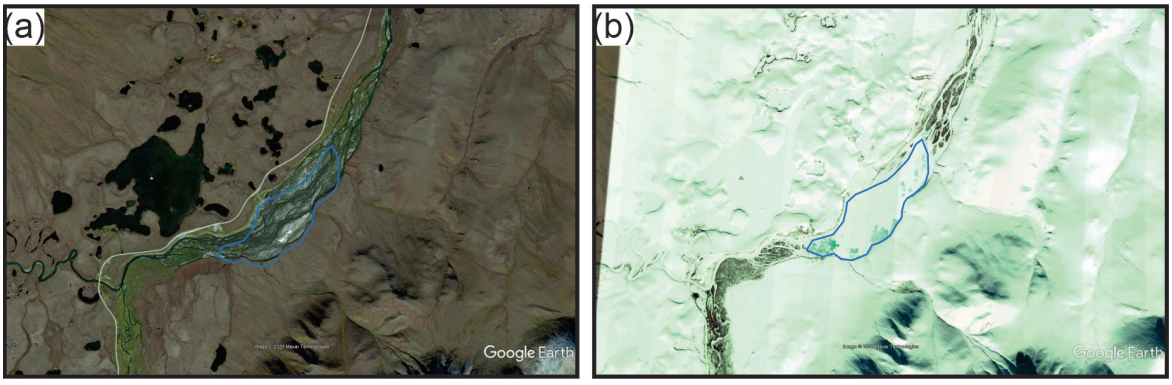

Figure 21. An icing location on the Blackstone River in the Ogilvie Mountains (68.85°N, 138.31°W). Extent of icing is outlined in blue. (a) Icing area evident in August 2007 image by remnant ice, braided stream channels, and lack of vegetation. (b) April 2013 image of same location shows recent icing growth, denoted by areas of turquoise within the extent of the icing. Images from Google Earth™.

4.3.4 Lake / Pond Affected by Thermokarst

A lake affected by thermokarst, or thaw lake, commonly occupies a closed depression that formed from settlement of the ground following thawing of ice-rich permafrost or the melting of massive ice (Figure 22) (Harris *et al.*, 1988). Thermokarst lakes enlarge as thaw of ice-rich permafrost subjacent to the shoreline causes lake-bottom settlement and shoreline collapse, a process sometimes leading to development of retrogressive thaw slumps (Kokelj *et al.*, 2009). Thermokarst lakes commonly develop in fluvial terraces, outwash plains, coastal areas, and drained-lake basins (French, 2007). The shoreline may be smooth (French, 2007) or show signs of instability, such as block failures, shoreline slumping, retrogressive thaw slumps, toppling of trees, other vegetation and soil, and incorporation of polygonal ponds in areas with abundant ice wedges.

Oriented lakes in permafrost terrain commonly have an elongate form and share a systematic orientation with surrounding lakes (French, 2007). The oriented forms include oval, elliptical, rectangular, triangular, and clam-shaped. The long axes are often oriented perpendicular to the prevailing winds, however, the cause of the orientation is not clear. Oriented lakes can be thaw lakes if they meet the criteria mentioned above.

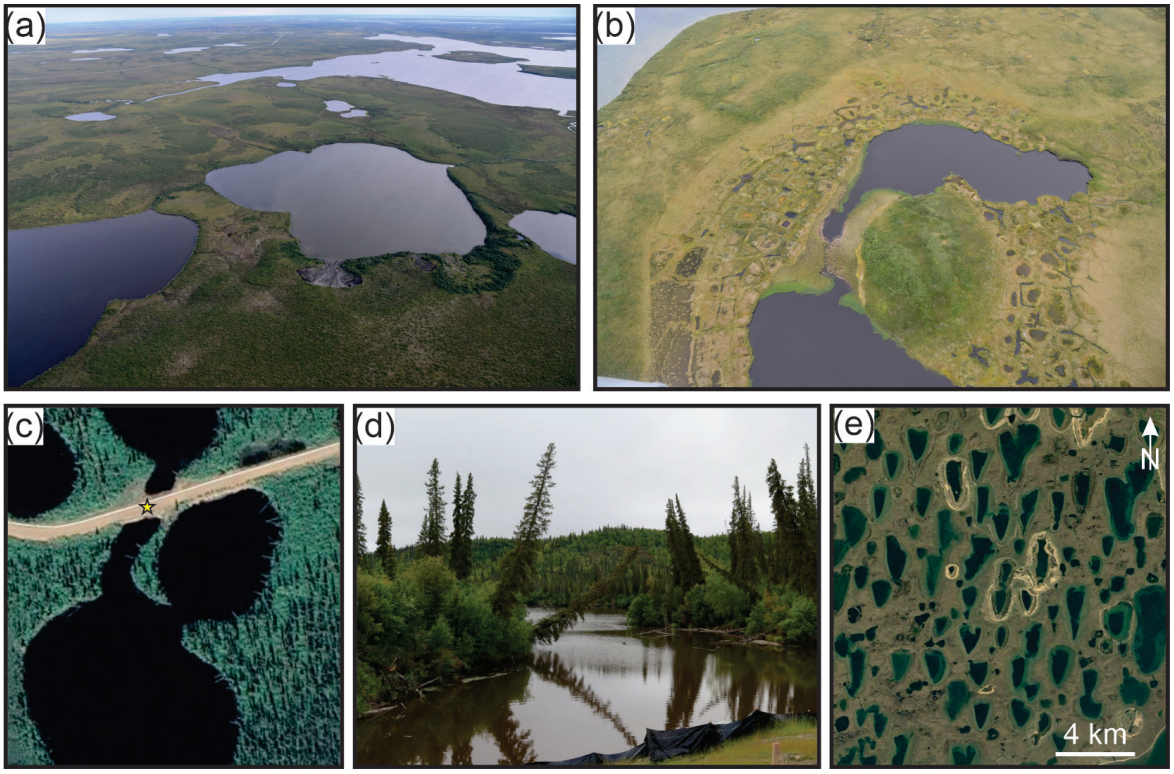

Figure 22. (a) Thermokarst activity indicated by presence of retrogressive thaw slumps along shoreline of a small tundra lake north of Noell Lake (68.60°N, 133.61°W) (Photograph by P.D. Morse. NRCan photo 2020-230). (b) Thermokarst activity indicated by presence of degrading ice wedges along the shoreline, northeast of Tuktoyaktuk (69.54°N,132.40°W) (Photograph by P.D. Morse. NRCan photo 2020-231). (c) Aerial image of fallen trees along collapsing shoreline in the alluvial deposits of the Peel Plain, south of Fort McPherson (67.33°N, 134.91°W) (image from Google Earth™). (d) Tilted trees along the collapsing shoreline viewed from Dempster Highway at the star in (c) (Photograph by P.D. Morse. NRCan photo 2020-232). (e) Example of oriented lakes on the Tuktoyaktuk Peninsula with long axes aligned north-south (69.94°N, -130.23°W) (image from Google Earth™).

4.3.5 Thermokarst Gully

Thermokarst gullies result from the thermal erosion of channelized surface water into ice-rich soils (Fortier *et al.*, 2007). These features are commonly associated with ice-wedge polygon networks because the troughs provide natural flow paths underlain by wedge ice (Kokelj and Jorgenson, 2013). Gully development in polygonal terrain may lead to formation gully networks (Fortier *et al.*, 2007) or rapid lake drainage (Mackay, 1988). Initiation of thermokarst gullying may be partially due to anthropogenic concentration of surface water, such as at culverts (McKillop *et al.*, 2016).

A thermokarst gully may be identified as having a steep-sided trench or channel surface expression (Godin and Fortier, 2012). Sinkholes and retrogressive thaw slumping may be visible along the gully. These gullies are commonly incised 1 – 5 m and may extend for hundreds of metres (Kokelj and Jorgenson, 2013). Thermokarst gullies may be found within an ice-wedge polygon network (Figure 23); along sides of earthflows/valley infills where they may lead to secondary slumps and valley thaw slump complexes with multiple lobes; or extend from a drained-lake basin or a linear structure (e.g., road culverts).

Figure 23. Thermokarst gully examples in the Tuktoyaktuk Coastlands. (a) Thermokarst gully on Beaufort Coast (70.02°N, 129.53°W) (Photograph by P.D. Morse. NRCan photo 2020-233). (b) Two thermokarst gullies shown: one leading into a drained-lake basin along thawing ice wedges and one well-developed gully leading from the drained-lake basin (70.01°N, 129.50°W) (Photograph by P.D. Morse. NRCan photo 2020-234).

5 METHODOLOGY

5.1 Data

5.1.1 Satellite Imagery

The geomorphic feature digitizing methodology was developed using the most recent (2004-2018), high-resolution satellite imagery available for the 10-km swath of the DH and ITH. A combined total of 69 WorldView-2 (WV2), WorldView-3 (WV3), and GeoEye-1 (GE1) images were available for the snow-free months, covering the combined DH-ITH corridor (Figure 1). The wavelength and resolution for spectral bands are summarized in (Table 3). The discrepancy between WV2, WV3, and GE1 red and near-infrared bands affected the workflow but likely had no affect on the results, as the processed images were used for individual visual interpretation. The satellite images are listed in Appendix 1.

Table 3: Spectral band information for the satellite sensors.

Spectral band	GeoEye-1		WorldView-2 and WorldView-3	
	Range (nm)	Resolution (m)	Range (nm)	Resolution (m)
Panchromatic	450-800	0.6	450-800	0.6
Blue	450-510	2.4	450-510	2.4
Green	510-580	2.4	510-580	2.4
Red	655-690	2.4	630-690	2.4
Near infrared	780-920	2.4	770-895	2.4

5.1.2 Canadian Digital Elevation Model

The elevation data used in the orthorectification of the satellite imagery and creation of the 3D stereo-pairs are from the Canadian Digital Elevation Model (CDEM) (Government of Canada, 2018). This national-scale elevation raster dataset has a spatial resolution ranging from 0.75 x 0.75 arc seconds to 0.75 x 3.0 arc seconds, depending on latitude. The majority of the data used was south of 68°N and had a resolution of 0.75 x 0.75 arc seconds (about 20 x 20 m), while the data north of 68°N had a resolution of 0.75 x 1.5 arc seconds (about 20 x 50 m). The difference in resolution north and south of 68°N is presumed to have minimal effect on mapping results given its relative coarseness.

5.1.3 Supplementary Data

To support interpretation of geomorphic features, Northwest Territories Centre for Geomatics (NWTCG) provided high-resolution (1 m) elevation data derived from Light Detection and Ranging (LiDAR) data, collected in 2011, that covered the majority of the ITH corridor and the Peel Plateau section of the Dempster corridor (NWT Centre for Geomatics, 2017; van der Sluijs *et al.*, 2018). Similarly, one-metre resolution elevation rasters for approximately a 600-m swath of the Yukon portion of the Dempster corridor were provided by Geomatics Yukon (R. Gould, pers. comm., 2017).

5.2 Image Processing

Image processing required for feature digitization comprises pansharpening, orthorectifying, and generating stereo pairs from the raw data. Image processing and feature digitization uses ESRI® ArcMap™ and ArcPy™ library, PCI Geomatics® Geomatica® OrthoEngine®, and DAT/EM Systems International® Summit Evolution™ software, and related coding is in the Python® programming language version 2.7. The processing steps are outlined in Appendix 2.

5.2.1 Pansharpening of Raw Imagery

The raw satellite imagery is pansharpened to produce an enhanced natural colour, high-resolution multi-spectral image. Each raw satellite image included a 2.4-m resolution multi-spectral image set and a 0.6-m resolution panchromatic image set, each made up of a number of separate image tiles. The image tiles are mosaicked into a more manageable set of multi-spectral and panchromatic images, which are then used to generate pansharpened images. This is done using a batch processing model created in PCI Geomatica that stitches together the multi-spectral and panchromatic image tiles for a specific image to generate two mosaicked images (Option B, Appendix 2). The model then uses the PANSHARP tool to create an enhanced natural colour multi-spectral image with 0.6-m resolution using the blue, green, red, and near-infrared image bands as reference channels and the panchromatic image to increase the spatial resolution. This method is preferred as the PCI Geomatica's PANSHARP algorithm produces a superior pansharpened image compared with other image fusion methods

(Zhang, 2002a; 2002b). In cases when PCI Geomatica is not available, we use the Pansharpen tool in ArcMap with the orthorectified images for pansharpening (Option A, Appendix 2).

5.2.2 Orthorectification of Imagery

Two techniques are used to orthorectify the imagery and remove the distortion caused by topography (Appendix 2). The first, and quickest, technique utilises the GIS image metadata files (.IMD) (Option A). Prior to pansharpening (Section 5.2.1), the multispectral and panchromatic .IMD files are imported into ArcMap and orthorectified using the geometric function. When the .IMD files are not available, the second technique, which involves generating ground control points (GCPs) manually in ArcMap 10.2 for each pansharpened image, is used (Option B). The GCP selection method corresponds to the best available data for each image. The most accurate method involves matching a point on the image to a point on a feature in the 1:50 000 scale CanVec waterbody layer (Government of Canada, 2018). This requires the image to have a good distribution of waterbody features across it. The second method uses the 1:50 000 scale CanVec watercourse layer (Government of Canada, 2018). This method is considered less accurate as the location of small streams often appeared generalized, making it difficult to select the associated point on the image. If there are almost no water features in an image, GCPs are created from orthorectified, high-resolution satellite and aerial images from Geomatics Yukon (GY) and NWTCG web service layers (Geomatics Yukon, 2018; NWT Centre for Geomatics, 2018). Distinct features that appear in both images are selected and paired with the control points. This third method is time consuming and often yields less accurate results than the water feature methods so it is used as a last option. Once 15 to 20 evenly distributed GCPs are placed on an image, the table of residuals are examined and any GCP that had a residual higher than the specified cut-off value is removed. The residual cut-off value for the GCPs are determined based on the type and spatial distribution of the data available for each image (Table 4). If necessary, additional control points are selected until the image contains a minimum of ten evenly distributed GCPs with acceptable residuals.

Table 4: Ground control point (GCP) cut-off values based on type and spatial distribution of the data available for orthorectification.

Type and Distribution	Cut-off Value
Good distribution of vector data across the image	< 10 m
Poor distribution of vector data across the image	< 15 m
Good distribution of raster data across the image	< 20 m
Poor distribution of raster data across the image	< 30 m

A custom-built Python tool integrated into ArcGIS converts the GCPs into IPLXYE format (Appendix 3). This tool converts the portion of the each GCP tied to the image from UTM coordinates to pixel row and column numbers in the image. It then formats and exports the converted file. The converted GCPs along with the corresponding imagery and the CDEM are then imported into OrthoEngine to generate the orthorectified image. Since the DH occurs in both UTM zone 7 and 8, but the majority of the highway is in zone 8, the orthorectified images located in UTM zone 7 are reprojected to zone 8 so that all the imagery is in the same projection. Lastly, each image is individually colour corrected to facilitate and enhance feature identification and digitization.

5.2.3 Three-dimensional Image Generation

To view the imagery in 3D, stereomates (synthetic stereo image pairs) are generated for all of the images using Summit Evolution (DAT/EM). The orthorectified images and CDEM are imported into Summit's Stereomate Creator. Stereomates are generated using a shift of one ground-per-pixel (gpp) in images covering areas with low to moderate elevation variation, a shift of 0.5 gpp is used for images covering areas with extreme variation in elevation, such as in mountainous regions.

5.3 Feature Digitization and Attribute Extraction

Features are identified visually using the 3D imagery in Summit and complementary data, such as LiDAR and surficial geology maps, in ArcMap. Features are digitized if they meet a series of criteria (Appendix 4). ArcMap and Summit automatically synchronize with each other allowing the vector data in ArcMap to be overlaid on the 3D image in Summit. The features are digitized in 3D and saved directly to the feature database open in ArcMap. The feature database consists of three line layers and three point layers, one for each process class: mass movement, periglacial, and hydrological. Feature polygons are generated using the digitized the feature extent (line layer) and the feature-type point (point layer) within the feature extent. User-defined attributes are assigned to the feature point (Table 5). A series of custom-built Python scripts, which employ the ArcPy library, convert the data from the points and lines into polygons and complete the attribute tables (Appendix 3). Table 5 lists the attribute fields, descriptions, input method, and source if applicable. The polygon and attribute data are manually inspected for quality control. The metadata are attached to the data layers to create the final product.

Table 5. Attribute fields, descriptions, generation method, and source.

Field	Description	Input method	Source
OBJECTID	Unique identification number	Autogenerated	
LAT	Latitude of feature centroid	Calculated	
LONG	Longitude of feature centroid	Calculated	
NTS_50K	National Topographic System map number	Joined from source	Government of Canada, 2018
CLASS	Feature class	Derived	
TYPE	Feature type	User-defined	
SUBTYPE	Feature subtype, if applicable	User-defined	
SUBTYPE_DESC	Feature subtype description, if applicable	User-defined	
IND_MUL	Individual vs. multiple features	User-defined	
ACTIVITY*	Active vs. inactive	User-defined	
MATERIAL*	Feature material	User-defined	
ORIENTED†	Similar orientation as surrounding features	User-defined	
AREA_HA	Feature area in hectares	Calculated	
COMMENTS	Comments by mapper	User-defined	
SURF_GEOL	Surficial geology unit	Joined from source	Duk-Rodkin and Hughes, 1992a,b; 1992b; Rampton, 1988; Thomas and Rampton, 1987a,b,c,d,e,f
PHYS_REG	Physiographic region/subdivision	Joined from source	Bostock, 1970; Mathews, 1986; Rampton, 1988
PF_DESC	Permafrost zone	Joined from source	Heginbottom *et al.*, 1995
IMG_SET	Image set	Joined from source	Digital Globe, 2018
IMG_NUM	Image number	Joined from source	Digital Globe, 2018
IMG_DATE	Date of image	Joined from source	Digital Globe, 2018
IMG_SOURCE	Source of imagery	Joined from source	Digital Globe, 2018

* Pertains to mass movement features only. † Pertains to hydrological features only.

5.4 Site Selection

We selected five 10 x 20 km test areas to represent the variety of terrain traversed by the DH-ITH. These are located in the (1) Ogilvie Mountains, (2) Eagle Plain, (3) Peel Plateau, (4) Anderson Plain, and (5) Tuktoyaktuk Coastlands (Figure 1). These test sites span a wide range of permafrost, geomorphic, and bio-climatic conditions and provided a comprehensive range of features allowing for refinement of feature identification methods and the classification scheme.

5.5 Quality Control

Quality control is carried out at the feature identification and the polygon generation stages. This is necessary to ensure that features are consistently identified from mapper to mapper and delineated in a similar manner, and that polygons are produced for all digitized features.

5.5.1 Feature Identification

Feature identification quality control is conducted using a 2 x 2 km "status" grid generated for the entire study corridor. Each grid cell has a unique alpha-numeric identifier. A list of the manually assigned grid cell fields is in Table 6.

We selected several grid cells representative of the diverse terrain to calibrate the mapping criteria and train new mappers. Two mappers, at least one of which is an experienced mapper, individually digitize features following the identification criteria (Appendix 4) with results reviewed and compared. Similarities and differences in feature identification and digitization are discussed and if needed, mapping criteria refined. This method is repeated until there is consensus on both feature identification and digitization limits. As a compromise between the high-resolution of the imagery and the scale at which maps were to be produced, feature identification is typically at a scale of 1:10 000, and digitization at 1:5000.

The status grid is also used to track digitization progress of the study corridor. A *mapped* grid cell means all visible features have been digitized. A second mapper *checks* these cells and, if necessary, comments are added to grid cells containing questionable features for discussion with the original mapper or a senior mapper. The original mapper *reviews* the changes and comments and modifies any digitization as required. Once digitization within the grid cell is deemed satisfactory, the status is updated to *complete*.

Table 6. List of fields and their description for the cells in the status grid.

Field	Description
OBJECTID	Unique identification number
Shape	Grid cell shape: polygon
GRID_ID	Alpha-numeric identification per grid cell
STATUS	Grid cell mapping status (Mapped, Checked, Reviewed, Complete)
MAPPER	Name of mapper
CHECKED_BY	Name of reviewer
COMMENTS	Comments on grid cell feature digitization
DATE_COMPLETED	Date grid cell is revised
Shape_Length	Grid cell length
Shape_Area	Grid cell area

5.5.2 Polygon Generation

Quality control on feature polygon generation is carried out after the custom-built Python scripts are run to generate polygon layers of the digitized features. The attributes of the polygon layers are inspected to ensure that data are correct and that there are no missing, incorrect, or corrupted entries. Any anomalies are corrected in the associated point and line layers used to generate the polygons. In addition, the polygon layers are compared to the original point and line files to ensure that the Python script generates the polygons correctly from the digitized features. Discrepancies arise when digitized lines around a feature are not closed or if a point is missing within a feature. Any discrepancies are addressed in the line and point files and the polygon file is regenerated. The final polygon layers are then inspected at random to ensure the overall quality of the dataset.

6 TEST SECTION MAPPING PRELIMINARY RESULTS

The protocol test results are outlined below. Figure 24 to Figure 28 show the feature class spatial distribution among each test section. Figure 29 summarizes the feature class density per test section. Figure 30 to Figure 32 outline feature type distribution by test section.

Geomorphic feature distribution varies with physiographic region (Figure 29). The Tuktoyaktuk Coastlands contain the greatest number and density of permafrost geomorphic features by an order of magnitude compared to the other test sections. Periglacial feature density increases with latitude, reflecting the greater extent and diversity of ground ice north of Inuvik. Mass movement feature class dominates the Ogilvie Mountains and Peel Plateau test sections, the physiographic regions with the greatest relief along the corridor.

Lakes affected by thermokarst are the predominant hydrological feature in the Anderson Plain and Tuktoyaktuk Coastlands (Figure 30), reflecting the extensive ground ice and permafrost thaw-sensitivity of these northern physiographic regions. Beaded streams are the most common hydrological feature in the Eagle Plain, suggesting presence of icy valley sediments and polygonal terrain. Evidence of icings are only observed in the Ogilvie Mountains, likely related to the high relief in this physiographic region and an active groundwater system. Debris flow/fans are the main mass movement type in the Ogilvie Mountains and Eagle Plain, also reflecting the significant topographic relative relief in these areas (Figure 31). Rock glaciers and solifluction are common at high altitudes and are only found in the Ogilvie Mountains test site. Retrogressive thaw slumps dominate the mass movement feature type in the three northern test sites, indicating the presence of massive ground ice in glaciated permafrost terrain.

Ice-wedge polygons are the most common periglacial feature type mapped, with a general northward increase in aerial extent. No periglacial features are observed and mapped in the Ogilvie Mountains (Figure 32). String and net fens are found in the Anderson Plain and Tuktoyaktuk Coastlands, commonly associated with degrading polygonal peatlands in subarctic and low Arctic environments (Figure 32). Pingos are only observed in the Tuktoyaktuk Coastlands test section (Figure 32).

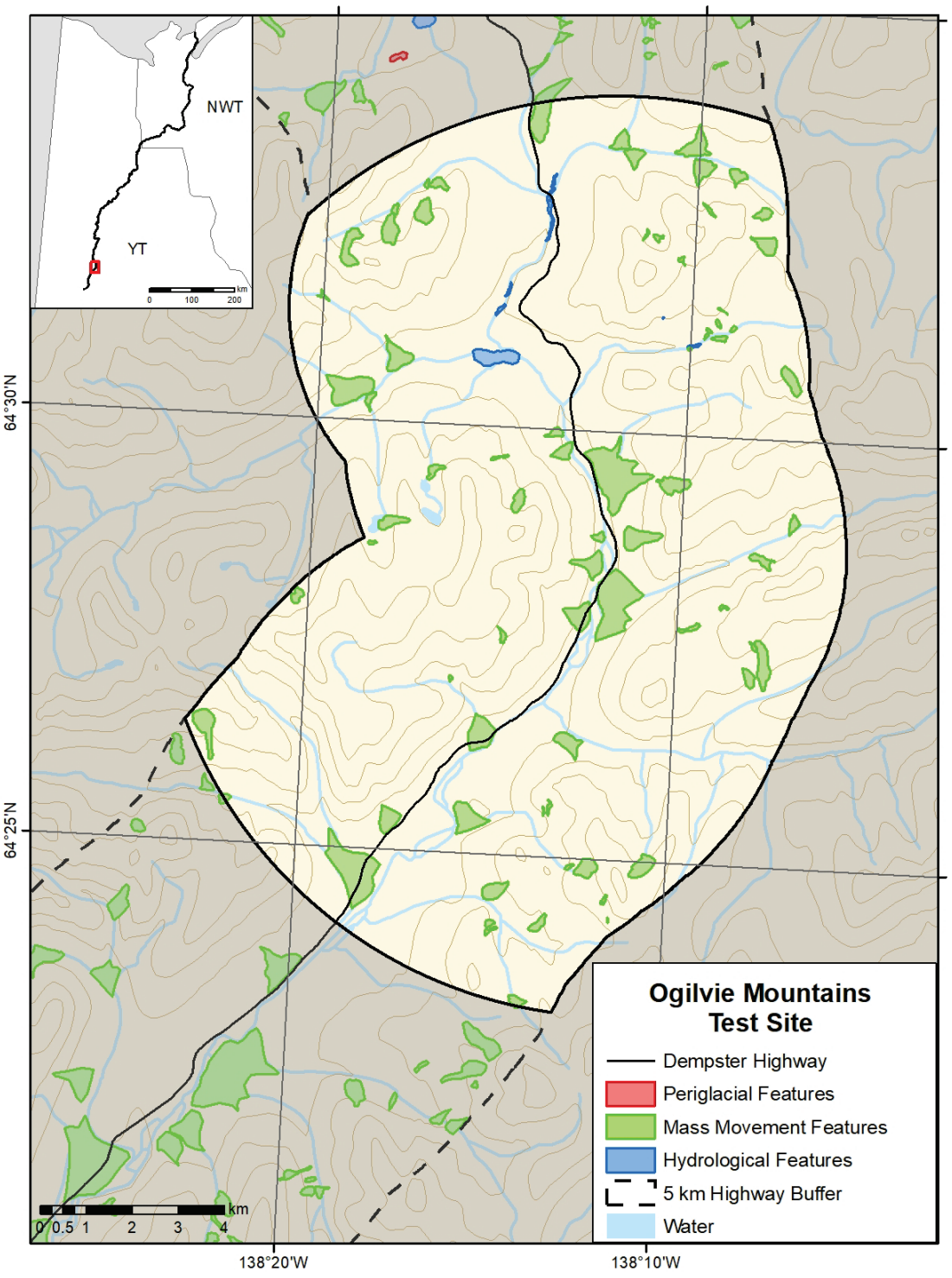

Figure 24. Digitized features in the Ogilvie Mountains test section, delineated by the highlighted area.

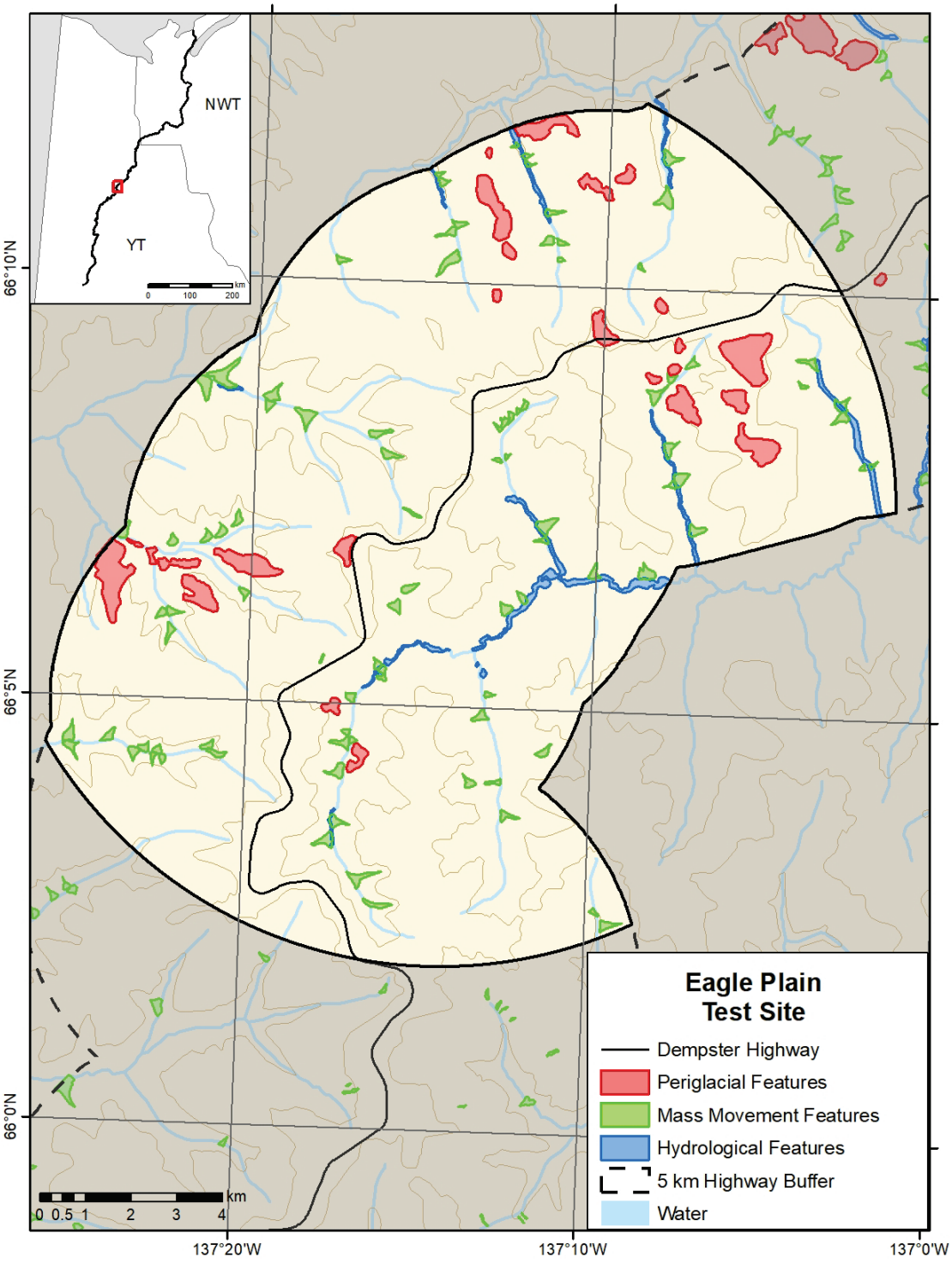

Figure 25. Digitized features in the Eagle Plain test section, delineated by the highlighted area.

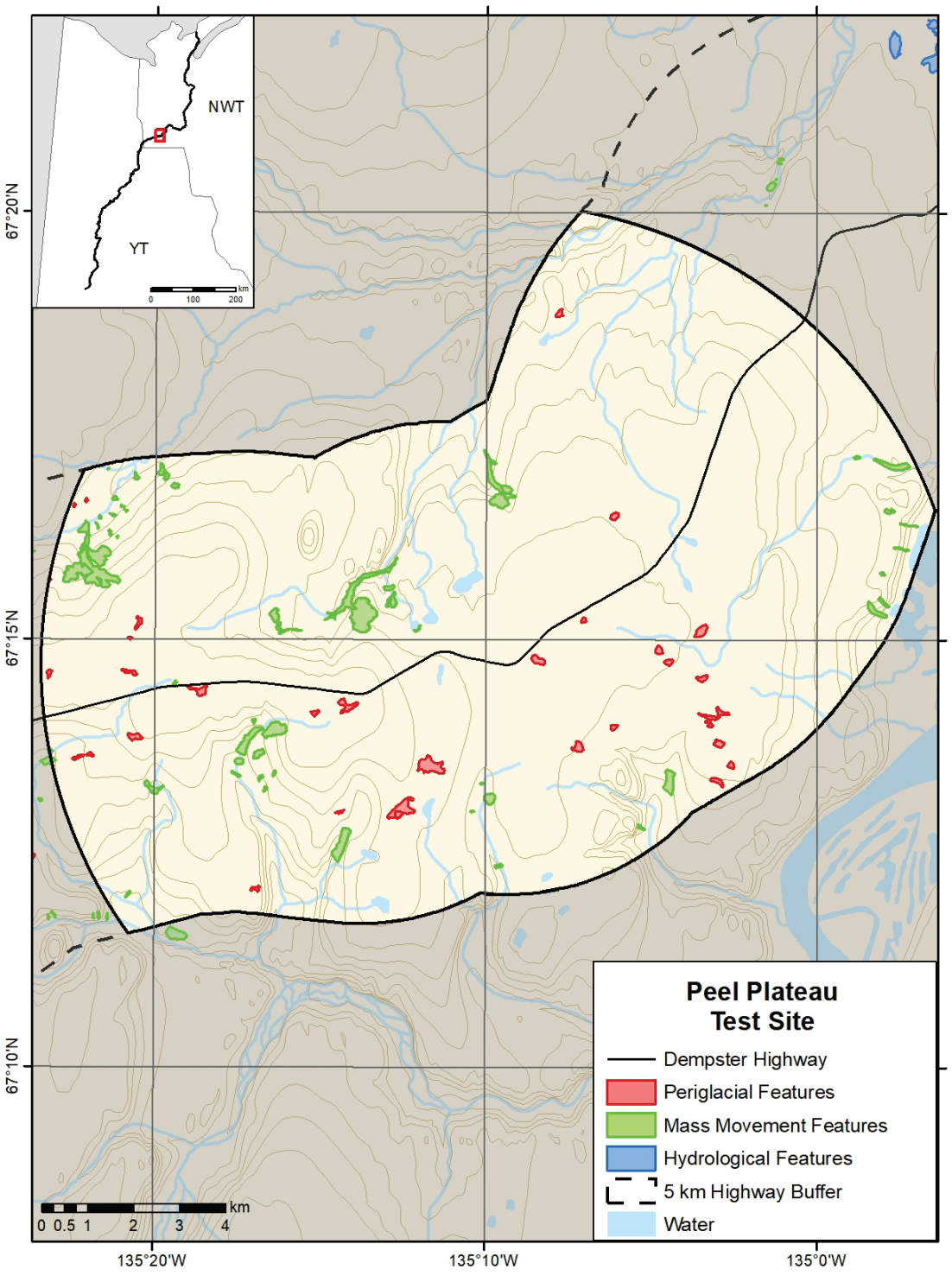

Figure 26. Digitized features in the Peel Plateau test section, delineated by the highlighted area.

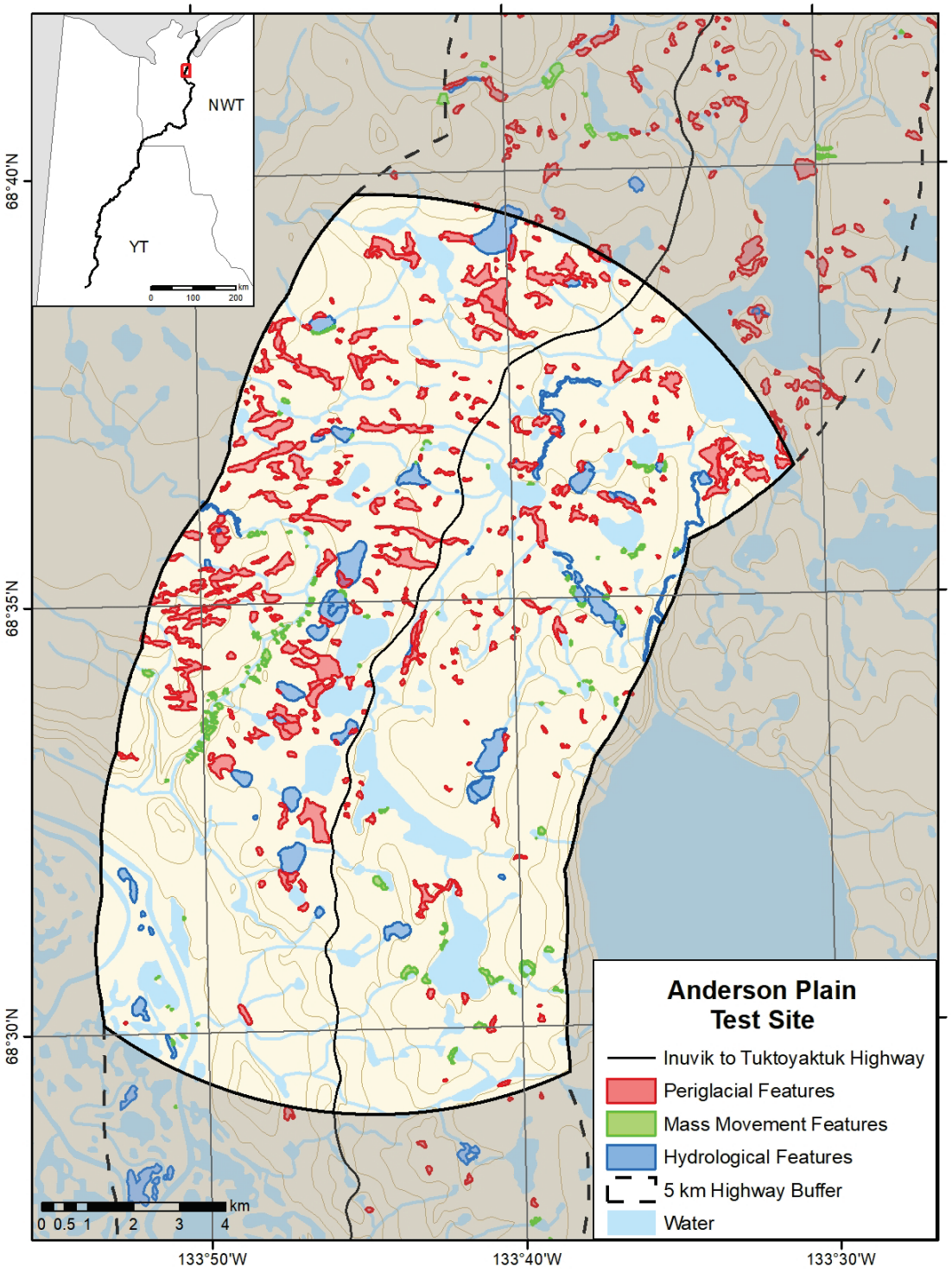

Figure 27. Digitized features in the Anderson Plain test section, delineated by the highlighted area.

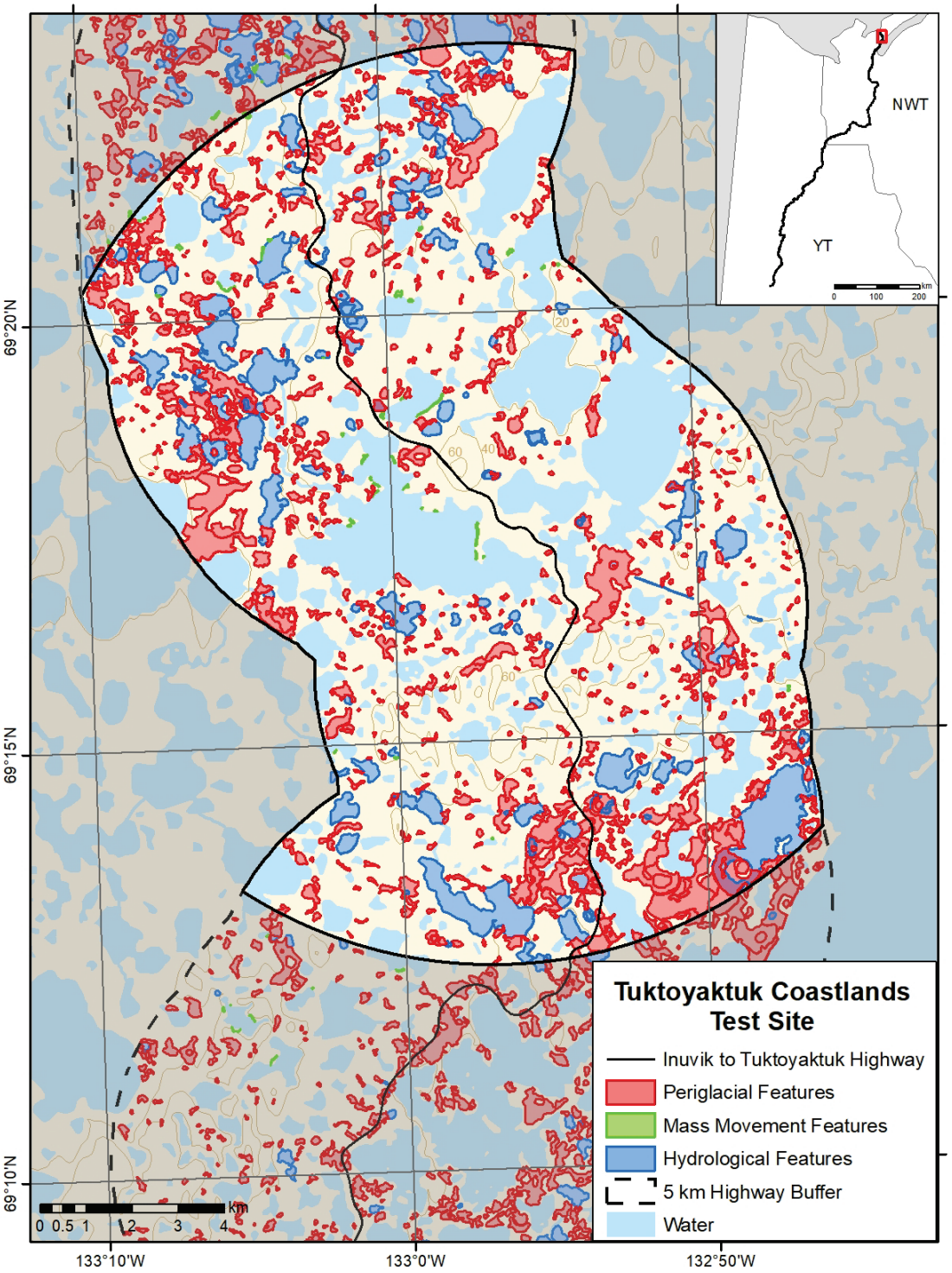

Figure 28. Digitized features in the Tuktoyaktuk Coastlands test section, delineated by the highlighted area.

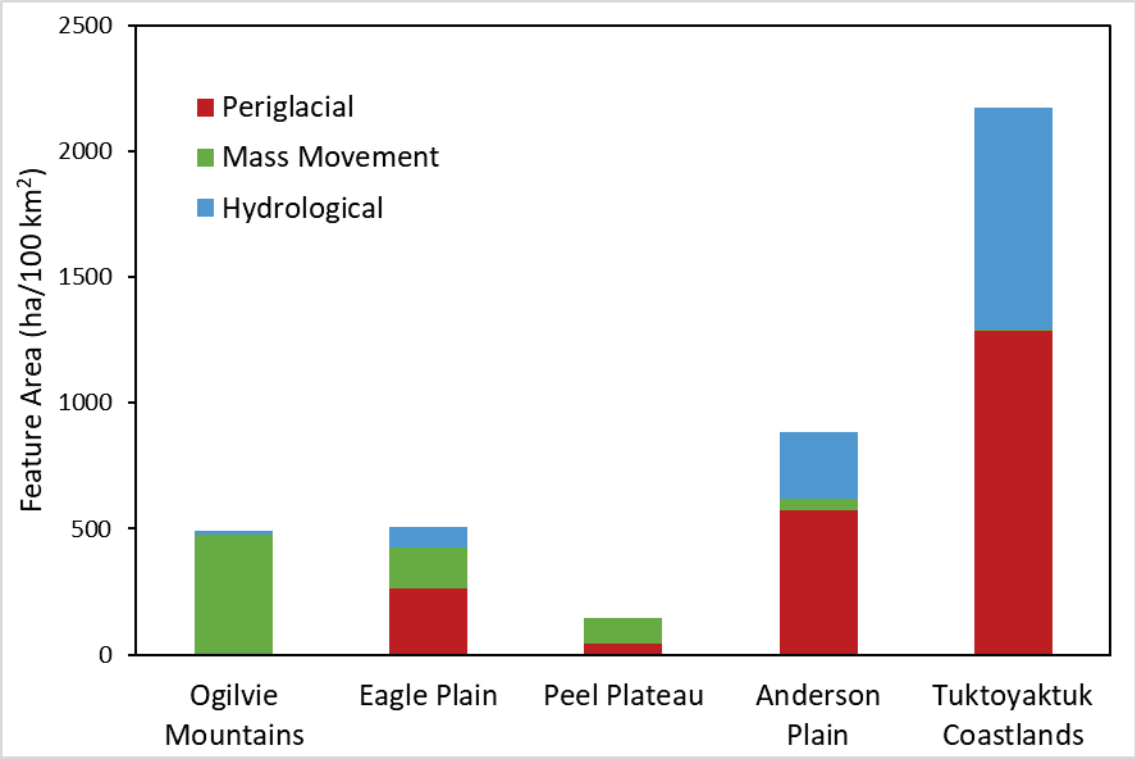

Figure 29. Summary of geomorphic feature class distribution by test area.

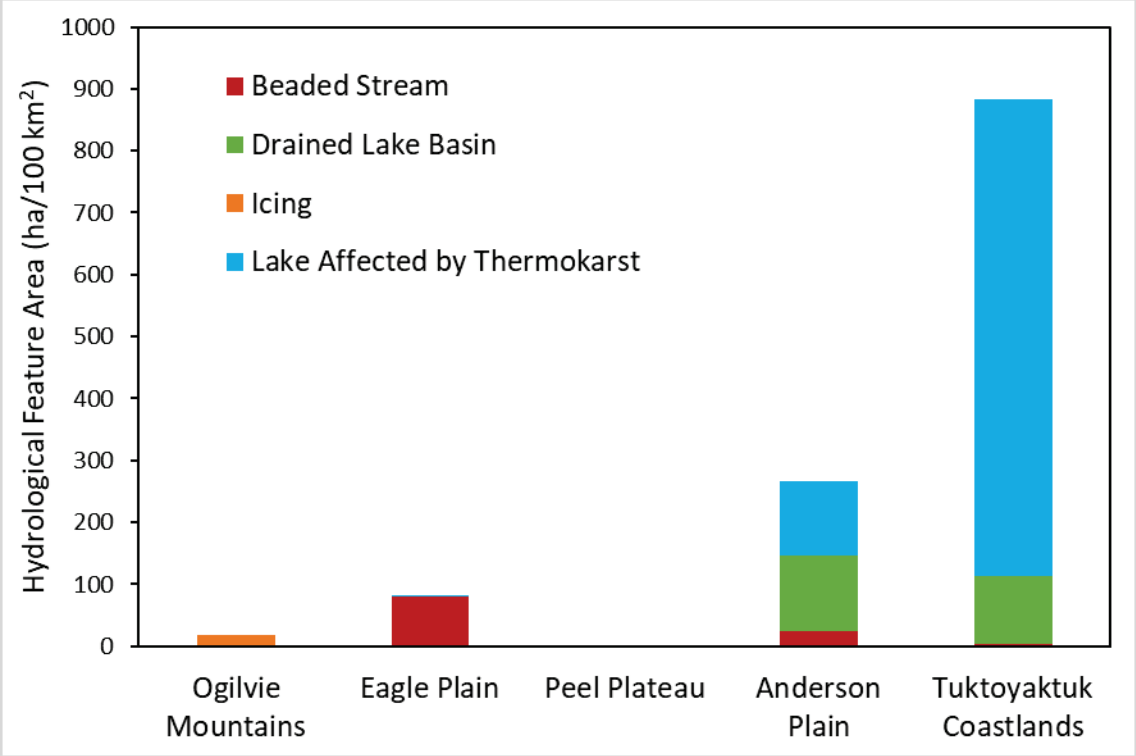

Figure 30. Hydrological feature type summarized by test area.

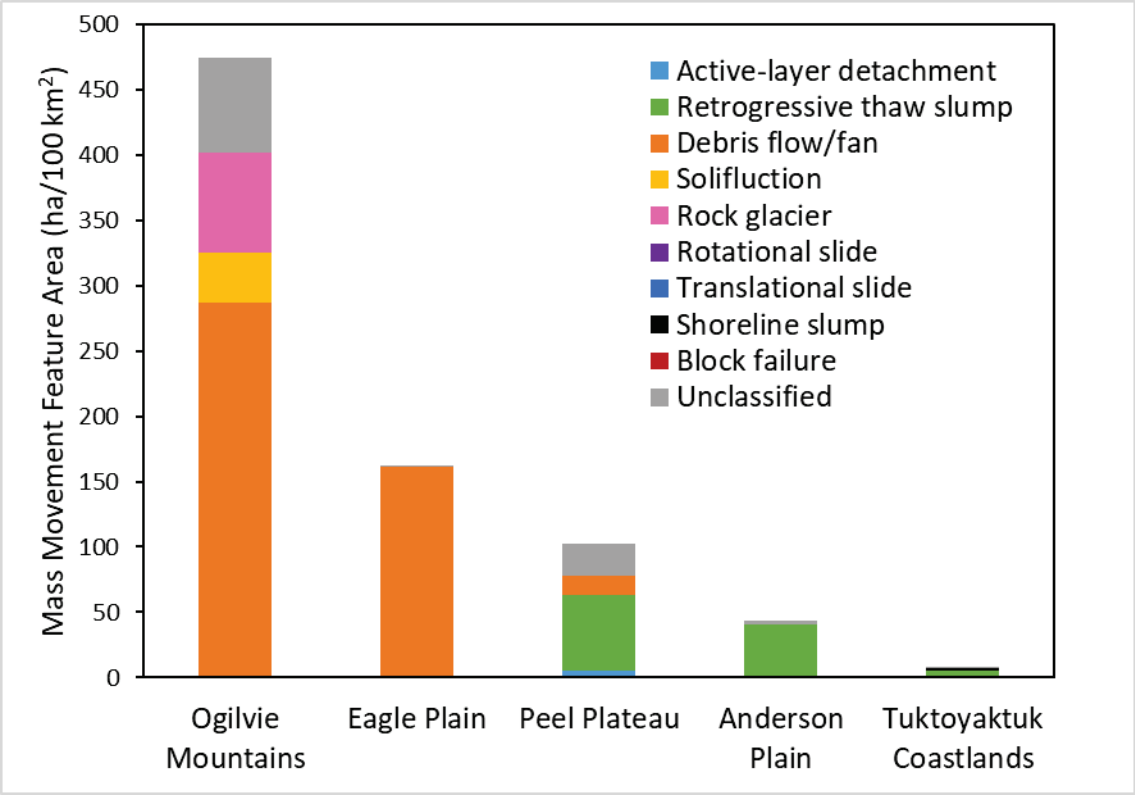

Figure 31. Mass movement feature subtype summarized by test area. Unclassified refers to mass movement features with undiscernible subtype features.

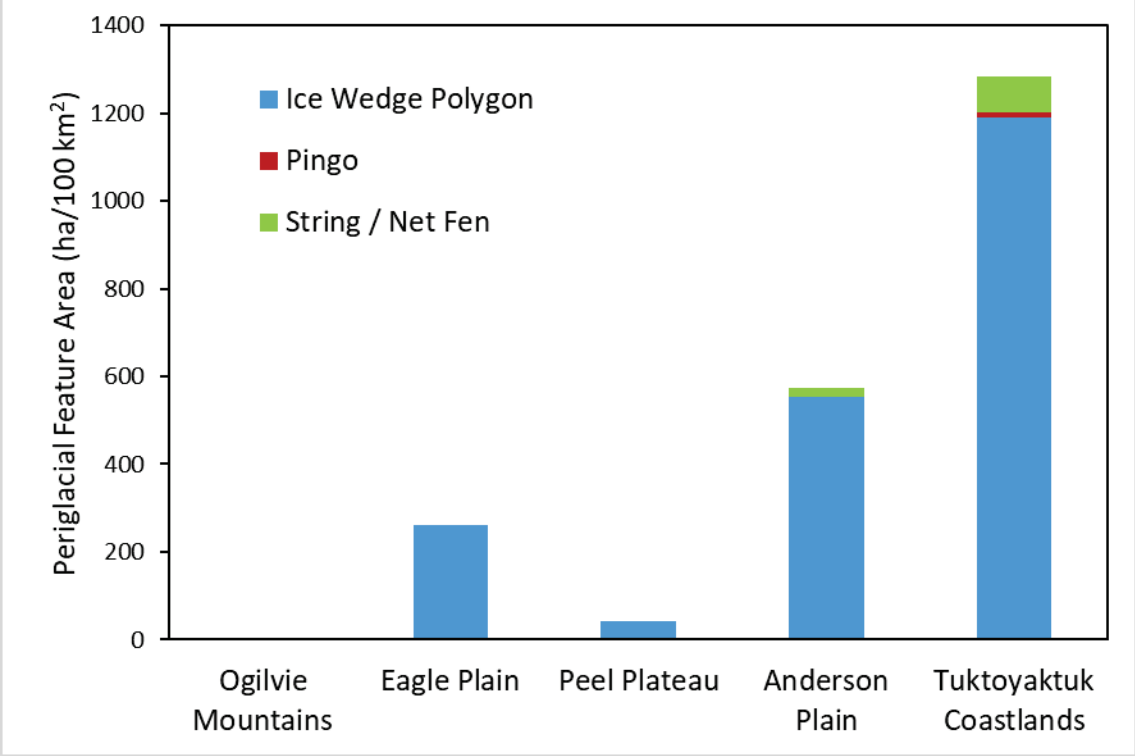

Figure 32. Periglacial feature type summarized by test area.

7 LIMITATIONS

7.1 Data Limitations

The main data limitation is that the best available elevation data that covers the entire DH-ITH corridor is the CDEM. The CDEM has a pixel size of approximately 20 m and the high-resolution imagery has a pixel size of 0.6 m. The mismatched resolution of the two datasets results in a number of issues for feature identification when the data are combined to generate the stereo pairs for 3D mapping. Features with local relief but with footprints at the same scale as the resolution of the CDEM data, such as pingos or palsas, do not appear in 3D, and therefore these features are more difficult to identify unless supplementary high resolution elevation data, such as LiDAR (van der Sluijs *et al.*, 2018), are available for the same area. In areas of low relief, such as along the ITH, the CDEM does not capture small-scale variation in elevation such as slightly elevated plateaus or shorelines. Lastly, several sections of the CDEM dataset are shifted by multiple pixels resulting in an offset between contours and features in the 3D imagery, such as streams that appear to run along the ridges beside valleys and hills in the middle of lakes. These issues result in difficulty identifying and/or delineating features. To compensate for the relatively coarse resolution of the CDEM, LiDAR data are consulted wherever available.

The bare earth LiDAR provides an excellent data set for delineating features that are obscured by vegetation. However, the extent of the LiDAR data is limited and does not cover the entire study corridor. As a result, it is used as reference supplementary data but was not used to generate the 3D imagery.

7.2 Mapping Limitations

Several limitations were encountered during the mapping. The first and most basic was human error during the feature identification and digitization stage. This is minimized by having mappers use the same feature identification criteria (Appendix 4) to standardize identification and digitization of features. In addition, all feature digitization is evaluated by at least a second mapper (see section 5.5). Lastly, where possible generation of attribute data is automated through Python script to reduce human error at the attribute input level.

The second mapping limitation encountered is where the ground is obscured due to cloud cover or shadow. Imagery with cloud cover is minimised because we obtained only those images with less than 10% cloud cover. The cloud cover is digitized and reported to account for the lack of features in the affected areas. Shadows are generally limited to areas of high relief such as the Ogilvie and Richardson mountains. Shadows obscure the ground and make it difficult to delineate features.

The third limitation are the breaks in imagery, in space and time. The imagery obtained for the study corridor is not continuous. In addition, due to size, most of the imagery is divided into sub-images to generate the 3D pairs. As a result, the study corridor can not be viewed continuously in Summit; only one image or sub-image can be viewed at a time. Therefore, features that straddle two images may have not been identified due to the disruption of loading images. In addition, date of imagery influenced identification of features such as icings.

The fourth limitation of mapping is the spatial accuracy of the features being mapped in the imagery, which stems from the orthorectification of the imagery. As previously discussed, the residual tolerance for GCPs varies based on the data used to orthorectify the image (Table 4). This issue is minimized by using the best available data to orthorectify each image and reducing the GCP residuals to the lowest possible values. However, where the best available data are poor, such as in areas with limited tie-in features, the high GCP residuals may have resulted in poor orthorectification of the

imagery. This was likely the case for a select number of images and therefore associated digitized features may not represent the actual geographic position of the feature on the ground.

The fifth limitation is that the mapping is carried out mainly as a desktop study. Field verification was conducted by aerial survey by helicopter and site visits by truck in summer 2018, but both were limited with respect to the entire study area. Features are identified primarily using the 3D imagery. However, the use of supplementary data sources is relied on heavily to compensate for the lack of field verification, including surficial and bedrock geology maps, LiDAR, and Northwest Territories Ecological Land Classification Photos (NWT Centre for Geomatics, 2017; 2019). In addition, we sought advice from experienced terrain mappers.

The final limitation is that certain features described in this protocol and known to occur in northern Canada were not observed and therefore not verified in this protocol. These include: thermokarst mounds, lithalsas, topples, and block failures.

8 SUMMARY

This Open File summarizes the methodology used to map geomorphological features related to mass wasting, periglacial, and hydrological processes in the periglacial environment. The study area is the 10-km wide corridor that follows the Dempster Highway and the Inuvik to Tuktoyaktuk Highway in the Yukon and Northwest Territories. The methodology is developed based on five test sections representative of the diverse physiography of the study corridor. The list of satellite imagery acquired for this project is provided in Appendix 1; the processing steps are outlined in Appendix 2; the custom Python script is found in Appendix 3; and the feature identification criteria are listed in Appendix 4.

A total of 1700 features are digitized across the five 10 x 20 km test areas located along the DH-ITH corridor. Slope and mass wasting features are most numerous in the Anderson Plain, however the Ogilvie Mountains have the greatest feature area per 100 km^2. Ground ice-related features and landforms are most common in the Tuktoyaktuk Coastlands followed by the Anderson Plain. These data can provide a basis of developing relationships between geomorphic features and landscape characteristics and a basis of developing spatial models of landscape susceptibility (e.g., Rudy *et al.*, 2019).

This Open File represents the first stage of feature identification and digitization along the Dempster Highway and Inuvik to Tuktoyaktuk Highway corridor. This work is ongoing and includes the digitization of features throughout the entire study corridor. Future work includes field verification; testing of the methodology for accuracy and replicability; and application of the methodology to other areas.

9 ACKNOWLEDGEMENTS

This work benefitted from discussions with Andrée Blais-Stevens, Janet Campbell, Dan Kerr, and Alain Plouffe of the GSC and Panya Lipovsky of the Yukon Geological Survey. Louis Robertson provided valuable consultation on the Summit software and digitization method. Erik Duncan, Sam Jardine, and Drew Branson helped with digitizing and figures. Jurjen van der Sluijs at NWT Centre for Geomatics provided bare earth LiDAR for sections of the corridor. Antoni Lewkowicz generously provided photographs of thermokarst mounds. Sharon Smith and Stephen Wolfe provided valuable feedback on the manuscript. Funding was provided by Natural Resources Canada's Climate Change Geoscience Program and Transport Canada.

10 REFERENCES

Aylsworth, J.M., Burgess, M.M., Desrochers, D.T., Duk-Rodkin, A., Robertson, T., and Traynor, J.A. 2000a. Surficial geology, subsurface materials, and thaw sensitivity of sediments; *in* The physical environment of the Mackenzie valley, Northwest Territories: a base line for the assessment of environmental change, (ed.) L.D.Dyke and G.R. Brooks; Geological Survey of Canada, Bulletin 547, p. 41-48.

Aylsworth, J.M., Duk-Rodkin, A., Robertson, T., and Traynor, J.A. 2000b. Landslides of the Mackenzie valley and adjacent mountainous and coastal regions; *in* The physical environment of the Mackenzie valley, Northwest Territories: a base line for the assessment of environmental change, (ed.) L.D.Dyke and G.R. Brooks; Geological Survey of Canada, Bulletin 547, p. 167-176.

Bostock, H.S. 1948. Physiography of the Canadian Cordillera, with special reference to the area north of the fifty-fifth parallel; Geological Survey of Canada, Memoir 247, 106 p. DOI: 10.4095/103300

Bostock, H.S. 1970. Physiographic Subdivisions of Canada; *in* Geology and Economic Minerals of Canada; Queens Printer for Canada, Ottawa, Ontario, p. 9-30.

Burgess, M., Judge, A., Taylor, A., and Allen, V. 1982. Ground temperature studies of permafrost growth at a drained lake site, Mackenzie Delta; *in* Proceedings of the 4th Canadian Permafrost Conference, Calgary, (ed.) H. M. French; National Research Council of Canada, p. 3-11.

Burn, C.R. 2004. Permafrost; *in* Ecoregions of the Yukon Territory: Biophysical properties of Yukon landscapes, (ed.) C.A.S. Smith, J.C. Meikle, and C.F. Roots; Agriculture and Agri-Food Canada, PARC Technical Bulletin No. 04-01, Summerland, British Columbia, p. 32-35.

Burn, C.R. and Kokelj, S.V. 2009. The environmental and permafrost of the Mackenzie Delta area; Permafrost and Periglacial Processes, v. 20, p. 83-105. DOI: 10.1002/ppp.655

Burn, C.R., Moore, J.L., O'Neill, H.B., Hayley, D.W., Trimble, J.R., Calmels, F., Orban, S.N., and Idrees, M. 2015. Permafrost characterization of the Dempster Highway, Yukon and Northwest Territories; *in* Proceedings of the 7th Canadian Permafrost Conference, GeoQuébec 2015, Canadian Geotechnical Society, Québec, Québec, Paper 705.

Callaghan, T.V., Johansson, M., Anisimov, O., Christiansen, H.H., Instanes, A., Romanovsky, V., and Smith, S. 2011. Changing permafrost and its impacts; *in* Snow, Water, Ice and Permafrost in the Arctic (SWIPA); Climate Change and the Cryosphere, Arctic Monitoring and Assessment Program (AMAP), Oslo, Norway, chapter 5.

Catto, N.R. 1996. Richardson Mountains, Yukon-Northwest territories, 1974-9; Arctic, v. 51, p. 116-124.

Coultish, T.L. and Lewkowicz, A.G. 2003. Palsa dynamics in a subarctic mountainous environment, Wolf Creek, Yukon Territory, Canada; *in* Proceedings of the 8th International Permafrost Conference, Zurich, Switzerland, v. 1, p. 163-168.

Crites, H., Kokelj, S.V., and Lacelle, D. 2020. Icings and groundwater conditions in permafrost catchments of northwestern Canada; Science Reports, v. 10, article number 3283. DOI: 10.1038/s4198-020-60322-w

Cruden, D. and Varnes, D. 1996. Landslide Types and Processes; *in* Landslides Investigation and Mitigation, (ed.) A. Turner and R. Schuster; National Research Council, Washington, p. 36-75.

Digital Globe. 2018. Retrieved from Digital Globe: https://www.digitalglobe.com/ [accessed February 8, 2019]

Dixon, J., Dietrich, J.R., and MacNeil, D.H. 1992. Upper Cretaceous to Pleistocene sequence stratigraphy of the Beaufort-Mackenzie and Banks Island areas, Northwest Canada; Geological Survey of Canada, Bulletin 407, 90 p.

Duk-Rodkin, A. and Hughes, O.L. 1992a. Surficial geology, Fort McPherson-Bell River, Yukon-Northwest Territories; Geological Survey of Canada, Map 1745A, scale 1:250 000.

Duk-Rodkin, A. and Hughes, O.L. 1992b. Surficial geology, Arctic Red River, District Mackenzie, Northwest Territories; Geological Survey of Canada, Map 1746A, scale 1:250 000.

Duk-Rodkin, A. and Lemmen, D.S. 2000. Glacial history of the Mackenzie region; *in* The Physical Environment of the Mackenzie Valley, Northwest Territories: a base line for the assessment of environmental change, (ed.) L.D. Dyke and G.R. Brooks; Geological Survey of Canada, Bulletin 547, p. 11-20.

Dyke, L.D. 2000. Stability of permafrost slopes in the Mackenzie valley; *in* The Physical Environment of the Mackenzie Valley, Northwest Territories: a base line for the assessment of environmental change, (ed.) L.D. Dyke and G.R. Brooks; Geological Survey of Canada, Bulletin 547, p. 177-186.

Ecosystem Classification Group. 2007. Ecological Regions of the Northwest Territories – Taiga Plains; Department of Environment and Natural Resources, Government of the Northwest Territories, Yellowknife, Northwest Territories, 173 p.

Environment Canada. 2020. Canadian Climate Normals; Environment and Climate Change Canada, Government of Canada. <http://climate.weather.gc.ca/climate_normals> [accessed November 27, 2020]

Fortier, D., Allard, M., and Shur, Y. 2007. Observation of rapid drainage system development by thermal erosion of ice wedges on Bylot Island, Canadian Arctic Archipelago; Permafrost and Periglacial Processes, v. 18, p. 229-243.

French, H.M. 2007. The Periglacial Environment; John Wiley and Sons Limited, West Sussex, England, 458 p.

Gaanderse, A.J.R., Wolfe, S.A., and Burn, C.R. 2018. Composition and origin of a lithalsa related to lake-level recession and Holocene terrestrial emergence, Northwest Territories, Canada; Earth Surface Processes and Landforms, v. 43: 1032-1043. DOI: 10.1002/esp.4302

Geomatics Yukon. 2018. Web Maps and Data Services; Geomatics Yukon, Government of Yukon. <http://mapservices.gov.yk.ca/arcgis/rest/services/> [accessed March 1, 2018]

Gibson, C. M., L. E. Chasmer, D. K. Thompson, W. L. Quinton, M. D. Flannigan, and D. Olefeldt. 2018. Wildfire as a major driver of recent permafrost thaw in boreal peatlands. Nature Communications, v. 9, article number 3041.

Godin, E. and Fortier, D. 2012. Geomorphology of a thermo-erosion gully, Bylot Island, Nunavut, Canada; Canadian Journal of Earth Sciences, v. 49, p. 979-986.

Gordey, S.P., and Makepeace, A.J. 2003. Yukon digital geology (version 2); Geological Survey of Canada, Open File 1749, 2 CD-ROMs. DOI: 10.4095/214639

Government of Canada. 2018. Open Data; Government of Canada. <https://open.canada.ca/en/open-data> [accessed February 14, 2018]

Gray, J.T. and Seppälä, M. 1991. Deeply dissected tundra polygons on a glacio-fluvial outwash plain, Northern Ungava Peninsula, Québec; Géographie physique et quaternaire, v. 54, p. 111-117.

Green, L.H. 1972. Geology of Nash Creek. Larsen Creek, and Dawson map areas, Yukon Territory; Geological Survey of Canada, Memoir 364, 157 p. DOI: 10.4095/100697

Harris, S.A. 1993. Palsa-like mounds developed in a mineral substrate, Fox Lake, Yukon Territory; *in* Proceedings, Permafrost Sixth International Conference, 5-9 July 1993, Beijing, China, South China University of Technology Press, Wushan Guangzhan, China, p. 238-243.

Harris, S.A., French, H.M., Heginbottom, J.A., Johnston, G.H., Ladanyi, B., Sego, D.C., and van Everdingen, R.O. 1988. Glossary of permafrost and related ground-ice terms; National Research Council Canada, Technical Memorandum 142, 156 p.

Heginbottom, J., Dubreuil, M., and Harker, P. 1995. Canada – Permafrost; *in* The National Atlas of Canada, Natural Resources Canada, Geomatics Canada, Ottawa, Ontario, MCR Series no. 4177, scale 1:7 500 000.

Hu, X. and Pollard, W.H. 1997. The hydrologic analysis and modelling of river icing growth, North Fork Pass, Yukon Territory, Canada; Permafrost and Periglacial Processes, v. 8, p. 279-294.

Hughes, O.L. 1969. Distribution of open-system pingos in central Yukon Territory with respect to glacial limits; Geological Survey of Canada, Paper 69-34, 8p.

Hungr, O., Leroueil, S., and Picarelli, L. 2014. The Varnes classification of landslide types, an update; Landslides, v. 11, p.167-194.

Huscroft, C.A., Elliot, B.T., and Lipovsky, P.S. 2019. Permafrost and other periglacial landforms – Yukon Landform Atlas; Yukon Geological Survey, Yukon Government. <http://yukon2.maps.arcgis.com/apps/MapSeries/index.html?appid=c189e9906d404590b2865ba1b4b8d559> [accessed February 21, 2019]

Idrees, M., Burn, C.R., Moore, J., and Calmels, F. 2015. Monitoring permafrost conditions along the Dempster Highway; *in* Proceedings of the 7th Canadian Permafrost Conference, GeoQuébec 2015, Canadian Geotechnical Society, Québec, Québec, Paper 703.

Johnston, G.H. and Brown, R.J.E. 1965. Stratigraphy of the Mackenzie River Delta, Northwest Territories, Canada; Geological Society of America Bulletin 76, p. 103-112.

Judge, A.S., Pelletier, B.R., and Norquay, I. 1987. Permafrost base and distribution of gas hydrates; *in* Marine Science Atlas of the Beaufort Sea: Geology and Geophysics, Geological Survey of Canada Miscellaneous Report 40, Pelletier BR (ed.), 39 p.

Kokelj, S.V. and Burn, C.R. 2004. Tilt of spruce trees near ice wedges, Mackenzie Delta, Northwest Territories; Arctic and Alpine Research, v. 36, p. 615-623.

Kokelj, S.V. and Burn, C.R. 2005. Near-surface ground ice in sediments of the Mackenzie Delta, Northwest Territories, Canada; Permafrost and Periglacial Processes, v. 16, p. 291-303. DOI: 10.1002/ppp.537

Kokelj, S.V. and Jorgenson, M.T. 2013. Advances in thermokarst research; Permafrost and Periglacial Processes, v. 24, p. 108-119. DOI: 10.1002/ppp.1779

Kokelj, S.V., Jenkins, R.E.L., Milburn, D., Burn, C.R., and Snow, N. 2005. The influence of thawing permafrost on the water quality of small lakes across the forest-tundra transition, Mackenzie Delta region, Northwest Territories, Canada; Permafrost and Periglacial Processes, v. 16, p. 343–353.

Kokelj, S.V., Lacelle, D., Lantz, T.C., Tunnicliffe, J., Malone, L., Clark, I.D., and Chin, K.S. 2013. Thawing of massive ground ice in mega slumps drives increases in stream sediment and solute flux across a range of watershed scales; Journal of Geophysical Research: Earth Surface, v. 118, p. 681–692. DOI: 10.1002/jgrf.20063

Kokelj, S.V., Lantz, T.C., Wolfe, S.A., Kanigan, J.C., Morse, P.D., Coutts, R., Molina-Giraldo, N., and Burn, C.R. 2014. Distribution and activity of ice wedges across the forest-tundra transition, western Arctic Canada; Journal of Geophysical Research: Earth Surface, v. 119, p. 2032-2047. DOI: 10.1002/2014JF003085

Kokelj, S.V., Tunnicliffe, J.F., and Lacelle, D. 2017a. The Peel Plateau of Northwestern Canada: An ice-rich hummocky moraine landscape in transition; *in* Landscapes and landforms of Western Canada. (ed.) O. Slaymaker, Springer, Cham, p.109-122. DOI: 10.1007/978-3-319-4495-3_7

Kokelj, S.V., Tunnicliffe, J., Lacelle, D., Lantz, T.C., Chin, K.S., and Fraser, R. 2015. Increased precipitation drives mega slump development and destabilization of ice-rich permafrost terrain, northwest Canada; Global and Planetary Change, v. 129, p. 56-68. DOI: 10.1016/j.gloplacha.2015.02.008

Kokelj, S.V., Lantz, T.C., Kanigan, J., Smith, S.L., and Coutts, R. 2009. Origin and polycyclic behavior of tundra thaw slumps, Mackenzie Delta region, Northwest Territories, Canada; Permafrost and Periglacial Processes, v. 20, p. 173-184. DOI: 10.1002/ppp.642

Kokelj, S.V., Palmer, M.J., Lantz, T.C., and Burn, C.R. 2017b. Ground temperatures and permafrost warming from forest to tundra, Tuktoyaktuk Coastlands and Anderson Plain, NWT, Canada; Permafrost and Periglacial Processes, v. 28, p. 543-551. DOI: 10.1002/ppp.1934

Kokelj, S.V., Lantz, T.C., Tunnicliffe, J., Segal, R., and Lacelle, D. 2017c. Climate-driven thaw of permafrost preserved glacial landscapes, northwestern Canada; Geology, v. 45, p. 371-374. DOI: 10.1130/G38626.1

Lacelle, D., Bjornson, J., Lauriol, B., Clark, I.D., and Troutet, Y. 2004. Segregated-intrusive ice of subglacial meltwater origin in retrogressive thaw flow headwalls, Richardson Mountains, NWT, Canada; Quaternary Science Reviews, v. 23, p. 681-696. DOI: 10.1016/j.quascirev.2003.09.005

Lacelle, D., Brooker, A., Fraser, R.H., and Kokelj, S.V. 2015. Distribution and growth of thaw slumps in the Richarson Mountains-Peel Plateau region, northwest Canada; Geomorphology, v. 235, p. 40-51. DOI: 10.1013/j.geomorph.2015.01.024

Lantz, T.C., Kokelj, S.V., Gergel, S.E., and Henry, G.H.R. 2009. Relative impacts of disturbance and temperature: persistent changes in microenvironment and vegetation in retrogressive thaw slumps; Global Change Biology, v. 15, p. 1664-1675.

Lantz, T.C., Marsh, P., and Kokelj, S.V. 2013. Recent shrub prolifereation in the Mackenzie Delta Uplands and microclimatic implications; Ecosystems, v. 16, p. 47-59. DOI: 10.1007/s10021-012-9595-2

Lachenbruch, A.H. 1962. Mechanics of thermal contraction cracks and ice-wedge polygons in permafrost; Geological Society of America, Special Paper 70, 69 p.

Lawson, D.E. 1983. Erosion of perennially frozen stream banks; U.S. Army Corps of Engineers, Cold Region Research and Engineering Laboratory, Report 83–29, 22 p.

Lewkowicz, A.G. and Harris, C. 2005. Morphology and geotechnique of active-layer detachment failures in discontinuous permafrost, northern Canada; Geomorphology, v. 69, p. 275-297.

Lewkowicz, A.G., Bonnaventure, P.P., Smith, S.L., and Kuntz, Z. 2012. Spatial and thermal characteristics of mountain permafrost, northwest Canada; Geografiska Annaler Series A, Physical Geography v. 94, p. 153-162. DOI: 10.1111/j.1468-0459.2012.00462.x

Mackay, J.R. 1967. Permafrost depths, lower Mackenzie valley, Northwest Territories; Arctic, v. 20, p. 21-26.

Mackay, J. R. 1974a. Ice-wedge cracks, Garry Island, Northwest Territories; Canadian Journal of Earth Sciences, v. 11, p. 1366–1383. DOI: 10.1139/e74-133

Mackay, J.R. 1974b. The Mackenzie Delta area, N.W.T.; Geological Survey of Canada, Miscellaneous Report 23, 202 p.

Mackay, J.R. 1988. Catastrophic lake drainage, Tuktoyaktuk Peninsula area, District of Mackenzie; *in* Current Research, Part D; Geological Survey of Canada, Paper 88-1D, p. 83-90.

Mackay, J.R. 1992. Lake stability in an ice-rich permafrost environment: Examples from the Western Arctic Coast; *in* Arctic ecosystems in semi-arid regions: Implications for resource management, Saskatoon, (ed.) R.D. Robarts and M.L. Bothwell, N.H.R.I. Symposium Series 7, Environment Canada, p. 1-26.

Mackay, J.R. 1993. Air temperature, snow cover, creep of frozen ground, and the time of ice-wedge cracking, western Arctic coast; Canadian Journal of Earth Sciences, v. 30, p. 1720–1729. DOI: 10.1139/e93-151

Mackay, J.R. 1998. Pingo Growth and collapse, Tuktoyaktuk Peninsula Area, Western Arctic Coast, Canada: a long-term field study; Géographie Physique et Quaternaire, v. 52, p. 271-323. DOI: 10.7/202/004847ar

Malone, L., Lacelle, D., Kokelj, S., and Clark, I.D. 2013. Impacts of hillslope thaw slumps on the geochemistry of permafrost catchments (Stony Creek watershed, NWT, Canada); Chemical Geology, v. 356, p. 38-49. DOI: 10.1016/j.chemgeo.2013.07.010

Marsh, P., Russell, M., Pohl, S., Haywood, H., and Onclin, C. 2009. Changes in thaw lake drainage in the Western Canadian Arctic from 1950 to 2000; Hydrological Processes, v. 23, p. 145-158. DOI: 10.1002/hyp.7179

Mathews, W.H. 1986. Physiographic Map of the Canadian Cordillera; Geological Survey of Canada, Map 1701A, scale 1:5 000 000. DOI: 10.4095/122821

McKillop, R., Brown, C., McParland, D., Sacco, D., and Coates, J. 2016. Inventory of mass movement geohazards along the Dempster Highway, Yukon; Department of Energy, Mines and Resources, Government of Yukon, Whitehorse, Yukon, 248 p.

Mollard, J. and Janes, J. R. 1984. Airphoto interpretation and the Canadian landscape; Canadian Government Publishing Centre, Hull, Québec, 415 p.

Morse, P.D. and Wolfe, S.A. 2015. Geological and meteorological controls on icing (aufeis) dynamics (1985-2014) in subarctic Canada; Journal of Geophysical Research: Earth Surface, v. 120, p. 1670-1686. DOI: 10.002/2015JF003534

Nelson, F.E., Anisimov, O.A., and Shiklomanov, N.I. 2001. Subsidence risk from thawing permafrost; Nature, v. 410, p. 889–890. DOI: 10.1038/35073746

Norris, D.K. 1984. Geology of the Northern Yukon and Northwestern District of Mackenzie; Geological Survey of Canada, Map 1581A, scale 1:500 000.

Norris, D.K. (ed.). 1997. The geology, mineral and hydrocarbon potential of northern Yukon Territory and northwestern District of Mackenzie; Geological Survey of Canada, Bulletin 422, 401 p. DOI: 10.4095/208886

NWT Centre for Geomatics. 2017. Draft 1-m bare-earth digital terrain models of the Dempster Highway and Inuvik-to-Tuktoyaktuk Highway Corridors – Generated from 2011 Light Detection and Ranging (LiDAR) surveys conducted by McElhanney Consulting Services Ltd (version 1).

NWT Centre for Geomatics. 2018. Web Map Services (WMS); Northwest Territories Centre for Geomatics, Government of Northwest Territories. <www.geomatics.gov.nt.ca/wms.aspx> [accessed on March 1, 2018]

NWT Centre for Geomatics. 2019. Spatial Data Warehouse (SDW); Northwest Territories Centre for Geomatics, Government of Northwest Territories. <www.geomatics.gov.nt.ca/sdw.aspx> [accessed on February 21, 2019]

NWT Centre for Geomatics. 2020. Spatial Data Warehouse (SDW); Ecological Land Classification Photos; Photo_ID 163837; Northwest Territories Centre for Geomatics, Government of Northwest Territories. <www.geomatics.gov.nt.ca/elcphotos/compressed/Arctic%20Red%20Plain%20HS/NWT2005-07-22-001DSC_0474.JPG> [accessed on October 7, 2020]

O'Neill, H.B., Burn, C.R., and Kokelj, S.V. 2015. Field measurement of permafrost conditions beside the Dempster Highway embankment, Peel Plateau, NWT; *in* Proceedings of the 7th Canadian Permafrost Conference, GeoQuébec 2015, Canadian Geotechnical Society, Québec, Québec, Paper 380.

O'Neill, H.B., Wolfe, S.A., and Duchesne, C. 2019. New ground ice maps for Canada using a paleogeographic modelling approach. The Cryosphere, v. 13, p.753-773. DOI: 10.5194/tc-13-753-2019

Pissart, A. 2002. Palsas, lithalsas and remnants of these periglacial mounds: a progress report; Progress in Physical geography: Earth and Environment, v. 26, p. 605-621. DOI: 10.1191/0309133302pp354ra

Pissart, A. and French, H.M. 1976. Pingo investigations, north-central Banks Island, Canadian Arctic; Canadian Journal of Earth Sciences, v. 13, p. 937-946.

Rampton, V.N. 1988. Quaternary geology of Tuktoyaktuk Coastlands, Northwest Territories; Geological Survey of Canada, Memoir 423, 98 p.

Richardson, N.W. and Sauer, E.K. 1975. Terrain evaluation of the Dempster Highway across Eagle Plain and along the Richardson Mountains, Yukon Territory; Canadian Geotechnical Journal, v. 12, p. 296-319.

Roots, C. and Hart, C. 2004. Bedrock geology, *in* Ecoregions of the Yukon Territory: biophysical properties of Yukon landscapes; (ed.) C.A.S. Smith, J.C. Meikle, and C.F. Roots; Agriculture and Agri-Food Canada, PARC Technical Bulletin 04-01, p. 11-14.

Rudy, A.C.A., Morse, P.D., Kokelj, S.V., Sladen, W.E., and Smith, S.L. 2019. A new protocol to map permafrost geomorphic features and advance thaw-susceptibility modelling; *in* Proceedings of the 18th International Conference on Cold Regions Engineering & 8th Canadian Permafrost Conference, Québec, Québec, 11p.

Scudder, G.G.E. 1997. Environment of the Yukon; *in* Insects of the Yukon, (ed.) H.V. Danks and J.A. Downes; Biological Survey of Canada (Terrestrial arthropods), Ottawa, Ontario, p. 13-57.

Seppälä, M. 1982. An experiment study of the formation of palsas; *in* Proceedings of the 4th Canadian Permafrost Conference, Calgary, (ed.) H. M. French; National Research Council of Canada, p. 36-42.

Smith, C.A.S., Meikle, J.C., and Roots, C.F. (ed.). 2004. Ecoregions of the Yukon Territory: Biophysical properties of Yukon landscapes; Agriculture and Agri-Food Canada, PARC Technical Bulletin 04-01, Summerland, British Columbia, 313 p.

Steedman, A.E., Lantz, T.C., and Kokelj, S.V. 2017. Spatio-temporal variation in high-centre polygons and ice-wedge melt ponds, Tuktoyaktuk Coastlands, Northwest territories; Permafrost and Periglacial Processes, v. 28, p. 66-78.

Stumm, D., Schmid, M.O., Gruber, S., Baral, P., Shahi, S., Shrestha, T., and Wester, P. 2015. Manual for mapping rock glaciers in Google Earth; International Centre for Integrated Mountain Development (ICIMOD), Kathmandu, Nepal. <http://lib.icimod.org/record/31653> [accessed June 4, 2018]

Thomas, R.D. and Rampton, V.N. 1982a. Surficial geology and geomorphology North Klondike River, Yukon Territory; Geological Survey of Canada, Map 6-1982, 1:100 000.

Thomas, R.D. and Rampton, V.N. 1982b. Surficial geology and geomorphology Upper Blackstone River, Yukon Territory; Geological Survey of Canada, Map 7-1982, 1:100 000.

Thomas, R.D. and Rampton, V.N. 1982c. Surficial geology and geomorphology Engineer Creek, Yukon Territory; Geological Survey of Canada, Map 8-1982, 1:100 000.

Thomas, R.D. and Rampton, V.N. 1982d. Surficial geology and geomorphology Lower Ogilvie River, Yukon Territory; Geological Survey of Canada, Map 9-1982, 1:100 000.

Thomas, R.D. and Rampton, V.N. 1982e. Surficial geology and geomorphology Moose Lake, Yukon Territory; Geological Survey of Canada, Map 10-1982, 1:100 000.

Thomas, R.D. and Rampton, V.N. 1982f. Surficial geology and geomorphology Rock River, Yukon Territory; Geological Survey of Canada, Map 11-1982, 1:100 000.

USGS. 2007. North American elevation 1-kilometre resolution GRID; ScienceBase Catalog; United States Geological Survey. <www.sciencebase.gov/catalog/item/4fb5495ee4b04cb937751d6d > [accessed October 22, 2020]

van der Sluijs, J., Kokelj, S.V., Fraser, R.H. Tunnicliffe, J., and Lacelle, D. 2018. Permafrost terrain dynamics and infrastructure impacts revealed by UAV photogrammetry and thermal imaging; Remote Sensing, v. 10, article number 1734, 30 p. DOI: 10.3390/rs10111734

Vincent, W.F., Callaghan, T.V., Dahl-Jensen, D., Johansson, M., Kovacs, K.M., Michel, C., Prowse, T., Reist, J.D., and Sharp, M. 2012. Ecological Implications of Changes in the Arctic Cryosphere; Ambio, v. 40, p. 87–99. DOI: 10.1007/s13280-011-0218-5

Walker, H.J. and Arnborg, L. 1963. Permafrost and ice wedge effect on riverbank erosion; *in* Proceedings of the First International Conference on Permafrost, U.S. National Academy of Science Press, Washington, D.C., p. 164–171.

Warner, B.G. and Rubec, C.D.A. (ed.). 1997. The Canadian wetland classification system; National Wetlands Working Group, Wetlands Research Centre, University of Waterloo, Waterloo, Ontario, 68 p.

Washburn, A.L. 1980. Geocryology: a Survey of Periglacial and Environments; John Wiley and Sons, New York, U.S.A., 406 p.

Williams, P.J. and Smith, M.W. 1989. The Frozen Earth – Fundamentals of Geocryology; Cambridge University Press, Cambridge, New York, 306 p.

Wolfe, S.A., Stevens, C.W., Gaanderse, A.J., and Oldenborger, G.A. 2014. Lithalsa distribution, morphology and landscape associations in the Great Slave Lowland, Northwest Territories, Canada; Geomorphology, v. 204, p. 302-313.

Woo, M-k. 2012. Permafrost Hydrology; Springer-Verlag, Heidelberg, Germany, 564 p. DOI: 10.1007/978-3-642-23462-0

Yoshikawa, K., Hinzman, L.D., and Kane, D.L. 2007. Spring and aufeis (icing) hydrology in Brooks Range, Alaska; Journal of Geophysical Research, v. 112, G04S43, 14p. DOI: 10.1029/2006JG000294

Zhang, Y. 2002a. A new automatic approach for effectively fusing Landsat 7 images and IKONOS images; IEEE International geoscience and Remote Sensing Symposium, v. 4, p. 2429-2431.

Zhang, Y. 2002b. Problems in the fusion of commercial high-resolution satellite images as well as Landsat 7 images and Initial solutions; International Archives of Photogrammetry and Remote Sensing, v. 34, p. 587-592.

Zoltai, S.C. 1972. Palsas and Peat Plateaus in Central Manitoba and Saskatchewan; Canadian Journal of Forest Research, v. 2, p. 291-302.

Zoltai, S.C. and Tarnocai, C. 1975. Perennially frozen peatlands in the western Arctic and Subarctic of Canada; Canadian Journal of Earth Sciences, v. 12, p. 28-43.